

國立清華大學

碩士論文

研究粒線體酵素複合體 I 中 NDUFV2 次
單元的功能及其粒線體標的訊號

**The functional and mitochondrial targeting
signal studies of human NADH dehydrogenase
(ubiquinone) flavoprotein 2 (NDUFV2) subunit
in mitochondrial complex I**

所別: 分子醫學研究所

學號: 9680535

研究生: 劉欣瑜 Hsin-Yu Liu

指導教授: 高茂傑 Mou-Chieh Kao

中華民國九十八年七月

July 2009

Acknowledgments

首先要感謝我的指導教授高茂傑老師，在實驗上您總給我們最大的信任與支持，讓我們可以在科學研究的路上盡情的發揮自己的想法。也很謝謝周美智老師與張壯榮老師在論文及實驗上所提供的寶貴建議。

經由這次撰寫英文論文的過程中，讓我體驗到一篇科學文章的誕生是非常不容易的事，不僅實驗的部份要努力得到好結果之外，文章陳述時的邏輯性及一些專業要注意的細節都是非常重要的，真的很感謝高老師辛苦、仔細的給予指導修正，才能讓這本碩士論文能順利的完成。未來在科學研究的路上我一定會記取在清華所累積的經驗，希望自己能不斷的進步成長，絕不辜負老師們的栽培。

再來要感謝實驗室的夥伴們，若沒有他們的陪伴與支持也不會有今日的研究成果。謝謝俊仁學長在維持實驗室運作所付出的辛苦，謝謝博淳總像大哥一樣的照顧我們，也提供我許多電腦軟體相關的幫助，更要感謝定芳總給我許多實驗上寶貴的建議與協助，讓我的研究實驗可以順利的進行，另外要感謝我可愛的學弟妹們綢鈺、于廷及卉盈，他們不僅在研究上給予我很大的幫助，更在生活上帶給我很大的快樂，最後還要謝謝我的好朋友們瑩兒及婉慈，為我在清大的生活中增添許多難忘的回憶。

真的很感謝大家一直以來對我的照顧，我會好好珍惜這份情誼與緣份，更會帶著大家的祝福勇敢迎接未來的挑戰。

本實驗還要感謝財團法人罕見疾病基金會對於科學研究的支持與肯定，因為有你們的付出讓科學研究變得更有意義、更有價值，未來我們會繼續努力，希望能為社會及病友貢獻一己之力。

僅在此感謝財團法人罕見疾病基金會提供之
博碩士論文之獎助



中文摘要

NADH-ubiquinone oxidoreductase (complex I) 是粒線體呼吸鏈中最大且最複雜的酵素複合體。哺乳動物的 complex I 共含 45 個次單元，其中 7 個次單元是由 mitochondrial DNA (mtDNA) 所表現，其他的 38 個次單元則是由 nuclear DNA (nDNA) 表現後再經粒線體標的訊號(mitochondrial targeting signal, MTS)的帶領運送至粒線體。NADH dehydrogenase ubiquinone flavoprotein 2，簡稱 NDUFV2，則為 complex I 中由 nDNA 所表現的一個次單元，其含有一個[2Fe-2S]鐵硫中心，並於演化上具高度保留的特性。臨床上發現 NDUFV2 的缺失與一些神經退化性疾病有關，例如：帕金森氏症、阿茲海默症、躁鬱症及精神分裂症等。本實驗主要以 T-REx293 細胞為研究模式，針對 NDUFV2 的功能及其 MTS 進行系統性的研究。首先，利用核糖核酸干擾技術 (RNAi) 來抑制 *NDUFV2* 基因的表現，單純化探討 *NDUFV2* 在人類細胞中的功能。結果發現 *NDUFV2* 基因表現的下降會造成細胞有生長遲緩、耗氧能力下降、粒線體膜電位下降及自由基上升等表型，但 NDUFV2 的缺失並不影響 complex I 的組裝能力。由這些結果顯示 NDUFV2 對粒線體能量生成上扮演很重要的角色。另外，我們還定義了 NDUFV2 的 MTS 位於蛋白質 N 端及其被剪輯的切位位於第 32 個胺基酸，其中只需含有前 22 個胺基酸的片段即具有運送 enhanced green fluorescent protein (EGFP) 至粒線體的能力。隨後利用定點突變的方法探討 MTS 的序列訊號，結果發現鹼性及疏水性胺基酸對 NDUFV2 MTS 的運送功能很重要。實驗中我們還利用 T-REx293 細胞模擬早發性心肌腫大與腦病在臨床上所發現的 *NDUFV2* 基因剪輯異常的情形 (IVS2+5_+8delGTAA)，並從分子層次來研究 *NDUFV2* 基因缺失與此疾病的關係。結果發現上述突變正好破壞了 NDUFV2 的粒線體標的訊號，進而導致蛋白無法正確的被運送至粒線體執行其功能。本篇研究證實 NDUFV2 在粒線體能量生成的過程中扮演很重要的角色並定義了粒線體標的訊號所座落的位置及其重要性。

Abstracts

Mammalian NADH-ubiquinone oxidoreductase (complex I) is the first, largest and most complicated respiratory complex in mitochondria. Seven subunits of complex I, including ND1-6 and ND4L, are encoded by mitochondrial DNA (mtDNA), and the other thirty-eight subunits are encoded by nuclear DNA (nDNA). NADH dehydrogenase (ubiquinone) flavoprotein 2 (NDUFV2) is one of the core nucleus-encoded subunits existing in human mitochondrial complex I. It contains one iron sulfur cluster ([2Fe-2S] binuclear cluster N1a), which may play a role in the prevention of oxidative damage. The defect of NDUFV2 subunit is associated with neurodegenerative diseases, including Parkinson disease, Alzheimer's disease, Bipolar disorder and Schizophrenia. In this study, we applied the RNA interference (RNAi) technology in human T-REx293 cells to investigate the function of NDUFV2 subunit. We found that suppression of NDUFV2 expression in the cells would cause a slowing growth cell rate in galactose medium, decreasing oxygen consumption rate, reducing mitochondrial membrane potential (MMP) and increasing reactive oxygen species (ROS) generation, but did not affect complex I assembly. These observations provided the evidences that NDUFV2 plays an essential role for energy production in cells. In addition, we designed various truncation constructs to investigate the mitochondrial targeting mechanism of NDUFV2. We identified that the cleavage site of NDUFV2 was located around amino acid residue 32 and the first 22 residues of NDUFV2 was enough to function as a mitochondrial targeting sequence (MTS) to carry the passenger protein, enhanced green fluorescent protein (EGFP), into mitochondria successfully. Furthermore, we used the site-directed mutagenesis to study the basic, hydrophobic and hydroxylated residues in this identified N-terminal MTS. We found that the basic and hydrophobic residues were important for the MTS of NDUFV2, but

the hydroxylated residues were not. In a recent study, the patients of the hypertrophic cardiomyopathy and encephalomyopathy were found to contain 4 bp deletion in the second intron of *NDUFV2* (IVS2+5_+8delGTAA) to cause the exon 2 losing. To dissect the pathogenetic mechanism caused by this mutation, we established the human disease model and found that lost of this exon 2 cause *NDUFV2* to lose its mitochondrial targeting ability. In this report, we proved that the *NDUFV2* plays an important role for energy production in mammalian cells and identified the location of mitochondrial targeting sequence in this protein.



Table of Contents

Acknowledgments	i
中文摘要.....	iii
Abstracts	iv
Abbreviations	x
Introduction.....	1
Materials and methods	10
Results	17
<i>A. The functional studies of NDUFV2</i>	17
1. Reduced expression of NDUFV2 by RNAi.	17
2. Suppression of NDUFV2 expression in T-REx293 cells led to a slow grow rate in galactose containing medium.	17
3. The amount of oxygen consumption was decreased in NDUFV2 knock-down cells.	18
4. The suppression of NDUFV2 expression in T-REx293 cells decreased the MMP.	18
5. The suppression of NDUFV2 expression in T-REx293 cells increased the generation of ROS.	18
6. NDUFV2 dose not affect complex I assembly.	19
<i>B. Characterization of the mitochondrial targeting signal in NDUFV2</i>	19
1. The MTS of NDUFV2 was located at the N-terminus of the protein and its cleavage site was located around amino acid residue 32.	19
2. The N-terminal sequence of NDUFV2 including amino acids 1-22 could carry the EGFP to mitochondria.	21

3. Both basic and hydrophobic residues in MTS were very important for mitochondrial targeting of NDUFV2, but the hydroxylated residues were not.....	21
4. Establishing the human disease mechanism of the early-onset hypertrophic cardiomyopathy and encephalopathy.	22
Discussion.....	24
Tables.....	28
Figures.....	34
References	56
Appendixes.....	61



Figures

Figure 1. Multiple sequence alignment of NDUFV2 proteins from homologues	34
Figure 2. The RNAi effect on NDUFV2 mRNA and protein level	36
Figure 3. The growth rate of T-REx293 and NDUFV2 knock down 1F4 and 1F6 cell lines.....	37
Figure 4. Cellular oxygen consumption assay of T-REx293, 1F4 and 1F6 cells was measured by Mitocell S200 micro respirometry system.	38
Figure 5. Mitochondrial membrane potential of T-REx293, 1F4 and 1F6 cells was measured by FACS	39
Figure 6. ROS generation assay detecting the H₂O₂ levels in T-REx293, 1F4 and 1F6 cells	40
Figure 7. The hrCNE and complex I in gel assay were used to evaluate the assembly and activity of complex I.....	41
Figure 8. The effect of NDUFV2 N-terminal and C-terminal truncation on mitochondrial targeting.....	43
Figure 9. Cleavage site of the MTS occurs around residue 32 in the N-terminus of NDUFV2.....	44
Figure 10. The first N-terminal 22 amino acids of NDUFV2 are sufficient to serve as a MTS for mitochondrial import.....	47
Figure 11. The MTS of NDUFV2 is directional for mitochondrial import.....	48
Figure 12. The prediction of secondary and tertiary structure of NDUFV2....	50

Figure 13. The effect of hydroxylated residue mutation in NDUFV2 MTS	51
Figure 14. The effect of basic residue mutation in NDUFV2 MTS	52
Figure 15. The effect of hydrophobic residue mutation in NDUFV2 MTS	53
Figure 16. Establish the human early-onset hypertrophic cardiomyopathy and encephalopathy disease model.....	54
Figure 17. The prediction patterns of α helical wheel in NUHM₁₋₃₆ and truncated NUHM mutant.....	55



Abbreviations

NDUFV2: Human NADH dehydrogenase (ubiquinone) flavoprotein 2

RNAi: RNA interference

ETC: electron transport chain

OXPHOS: oxidative phosphorylation system

ATP: adenosine triphosphate

ADP adenosine 5'-diphosphate

Complex I: NADH-ubiquinone oxidoreductase

Complex II: succinate- ubiquinone oxidoreductase

Complex III: ubiquinol-cytochrome *c* oxidoreductase

Complex IV: cytochrome *c* oxidase

Complex V: ATP synthase

CoQ: ubiquinone

Cyt *c*: cytochrome *c*

MMP: mitochondrial membrane potential

ROS: reactive oxygen species

O₂^{•-}: superoxide anion radical

H₂O₂: hydrogen peroxide

•OH: hydroxyl radical

mtDNA: mitochondrial DNA

nDNA: nuclear DNA

MTS: mitochondrial targeting signals

EPR: electron paramagnetic resonance

TIM: translocase of the inner membrane

TOM: translocase of the outer membrane

EM: electron microscopy

cDNA: complementary DNA

bp: base pair

kDa: kilo-Dalton

MPP: mitochondrial processing peptidase

MIP: mitochondrial intermediate peptidase

DMEM: Dulbeccos modified Eagle medium

FBS: fetal bovine serum

RT-PCR: Semi-quantitative reverse-transcription polymerase chain reaction

Short hairpin RNA: shRNA

EGFP: enhanced green fluorescent protein

GAPDH: glyceraldehyde 3-phosphate dehydrogenase

PBS: phosphate-buffered saline

RB: respiration buffer

NTB: nitrotetrazolium blue

BSA: bovine serum albumin

SDS-PAGE: sodium dodecyl sulphate polyacrylamide gel electrophoresis

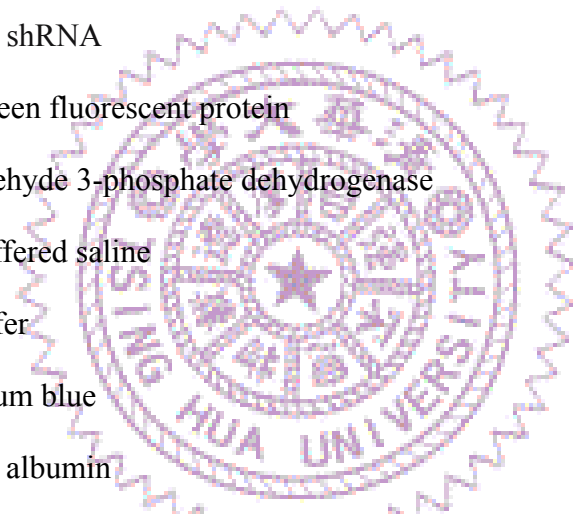
PVDF: polyvinylidene fluoride

ECL: enhanced chemiluminescence

carboxy-H₂DCFDA: 5-(and-6)-carboxy-2',7'-dichlorodihydrofluorescein diacetate

TMRM: tetramethylrhodamine methyl ester

HE: hydroethidine



Introduction

1. The structure of mitochondria

Mitochondria are the major energy producing organelles in the eukaryotic cells. They have dynamic shapes, sizes and numbers. Mitochondria have one special double-membrane structure: the outer membrane and the inner membrane (Appendix 1). There are five respiratory enzyme complexes located in the inner membrane to make up the electron transport chain (ETC) and oxidative phosphorylation system (OXPHOS) (Appendix 2). The space between these double membranes is the intermembrane space. The last compartment in mitochondria is called the matrix which is surrounded by the inner membrane and contains many important metabolic enzymes which are responsible for biochemical reactions like pyruvate oxidation, fatty acid β oxidation and tricarboxylic acid cycle etc.

2. Oxidative phosphorylation system (OXPHOS)

Mitochondria play many important roles in cells, including ATP synthesis, apoptosis and calcium homeostasis [1]. The most important functions of mitochondria is to convert the energy from redox reaction to the most common form, adenosine triphosphate, ATP [2]. In normal cells, 95 percent of ATP is produced by the OXPHOS, and just only 5 percent of this high energy compound is derived from glycolysis production. For this reason, the mitochondria are recognized as the powerhouse in cells [3]. These complicated biochemical reactions are carried out by five respiratory enzyme complexes and two mobile electron carriers. They are NADH-ubiquinone oxidoreductase (complex I), succinate-ubiquinone oxidoreductase (complex II), ubiquinol-cytochrome *c* oxidoreductase (complex III), cytochrome *c* oxidase

(complex IV), ATP synthase (complex V), ubiquinone (CoQ) and cytochrome *c* (Cyt *c*) (Appendix 2) .

In this energy transduction pathway, the electrons first enter complex I and II from NADH and succinate respectively, and are then delivered through electron carrier CoQ to Complex III. The electrons are further transferred via Cyt *c* to complexes IV and are finally accepted by oxygen to become water. In the OXPHOS, complexes I, III and IV use the redox energy to pump protons from the matrix side to the intermembrane space and establish the electrochemical proton gradient generating the mitochondrial membrane potential (MMP) which drives complex V to produce the ATP.

During the process of electron transfer, some electrons will be leaked out from the ETC and converted into unstable reactive oxygen species (ROS) such as superoxide anion radical ($O_2^{\cdot -}$), hydrogen peroxide (H_2O_2) and hydroxyl radical ($\cdot OH$), which may cause the oxidative damage of lipids, proteins and nucleic acids [4]. Complex I and III have been identified to be the major production sites of superoxide anions [5]. An imbalance between ROS production and removal in cells will cause the oxidative stress accumulation and lead to the decrease of mitochondrial antioxidant capacity the aging process [6]. The results of recent studies indicated that the OXPHOS dysfunction has been related to diabetes, age-related neurodegenerative diseases and cancers [7, 8].

3. The origin and genome of mitochondria

According to the endosymbiotic theory, mitochondria originate from the oxidative α -proteobacteria which are swallowed by the original proeukaryotes using endocytosis pathway. There are some evidences to support this theory and one of them

is that mitochondria contain their own genomic DNA, called mitochondrial DNA (mtDNA). These DNA molecules use the maternal mode of inheritance and some of their genomic codons are different from the universal codons used by the nuclear genes in eukaryotic cells. During the process of evolution, some of the genes located on the mtDNA are moved to the nucleus to become nuclear DNA (nDNA). Hitherto, only 37 genes encoded by mtDNA including 2 rRNA, 22 tRNA and 13 respiratory subunits are remained in mitochondrial genome [9]. Most mitochondrial proteins are encoded by nDNA and imported to the mitochondria with the help of mitochondrial targeting signals (MTS).

4. Mitochondrial targeting signals (MTS)

Recent studies have revealed that eukaryotic cells contain at least four mitochondrial import pathways [10]. They are as follows:

(1). Class I is presequence pathway

The general MTSs in this group lack a consensus sequence, but have some common features. Most mitochondrial matrix proteins contain a amino-terminal presequence with a positively charged amphipathic α -helix but lack of acidic amino acids. This presequence can direct the matrix proteins across the mitochondrial double membranes through the translocase of the inner membrane (TIM) and translocase of the outer membrane (TOM). After the proteins are imported into the matrix, the presequence are usually cleaved off by matrix proteinases [11, 12]. In addition, the mitochondrial targeting peptides contain some conserved cleavage motifs that the arginine (Arg) in positions -2, -3, -10 or -11 seem to be a recognition signal for the matrix proteinases [13].

(2). Class II is carrier pathway

Some of metabolite carriers such as the ADP/ATP carrier and phosphate carrier are required to be imported into the mitochondrial inner membrane. These carrier proteins usually contain six transmembrane segments and internal targeting signals. They are transported across the mitochondrial membranes through the TIM22-TOM complex with the guidance of the internal targeting signals which are difficult to identify and remain unknown.

(3). Class III is intermembrane space protein import pathway

The intermembrane space contains numerous cysteine motif proteins which are imported through the TOM complex and assembled by Mia40-Erv1-Hot13 pathway. Mia40 uses its cysteine motifs to recognize the intermembrane space precursor proteins through the disulphide bond interaction. Erv1, a sulphydryl oxidase, reoxidizes the Mia40 to make precursor proteins capable of assembling to become a oligomeric complex, and Hot13 plays a supporting role in the late steps of intermembrane space complex assembly.

(4). Class IV is outer membrane protein import pathway

The most outer membrane proteins are β -barrel proteins like porin and TOM40. These β -barrel proteins are translocated through the TOM complex and guided by TIM chaperone complex to SAM complex. Finally these unfolding precursors are converted to the β -barrel forms through MDM complex and Mim1 supporting.

5. The complex I of the mitochondria

Mammalian complex I is the first, largest and most complicated respiratory complex in mitochondria [14, 15]. Owing to its complexity only low-resolution electron microscopy (EM) structures are available for complex I [16]. This structure is L-shaped and separated into two arms: a hydrophobic arm embedded in the inner

membrane and a hydrophilic arm protruding into the matrix [17]. To date, 45 subunits of eukaryotic complex I have been identified from bovine heart mitochondria [18, 19]. Among them, seven subunits of complex I, including ND1-6 and ND4L, are encoded by mtDNA, and the others are encoded by nDNA [20].

Complex I is one of the electrons entry sites in the respiratory chain [21, 22]. It catalyzes NADH oxidation to transfer two electrons to ubiquinone. Bacterial complex I contains nine Fe-S clusters, including two [2Fe-2S] clusters (N1a and N1b) and seven [4Fe-4S] clusters (N3, N4, N5, N6a, N6b, N7 and N2), to manage the passage of these two electrons [23-25]. According to *Thermus thermophilus* model, N1a is in Nqo2; N3 and FMN are in Nqo1; N1b, N4, N5 and N7 are in Nqo3; N6a and N6b are in Nqo9; and N2 is in Nqo6. The electron transfer main pathway is NADH- FMN- N3- N1b- N4- N5- N6a- N6b- N2- quinone. Cluster N7 is suggested to be too far away from the other clusters to accept electrons and not present in many species. In contrast, cluster N1a can accept electrons from FMN, but is too far to donor electrons to N3. Therefore, they may not be part of the conserved electron transfer pathway [26].

6. The NDUFV2 subunit of mitochondrial complex I

Human NADH dehydrogenase (ubiquinone) flavoprotein 2 (NDUFV2) subunit, also called 24 kDa, is part of the complex I core subunits which are very conserved from bacteria to mammals [27]. *NDUFV2* gene is encoded by nDNA and located on chromosome 18p11.31-p11.2. The result from a recent study suggested that the promoter of *NDUFV2* gene lacks a TATA box or CAAT box, but contains three GC boxes under SpI transcription factor controlling [28, 29]. In addition, The NDUFV2 subunit is homologous to the NuoE of *Escherichia coli* [30] and *Rhodobacter*

capsulatus [31], NQO2 of *Paracoccus denitrificans* [32] and *Thermus thermophilus* [33], the nuo24 of *Neurospora crassa* [34] and the NUHM subunit of *Yarrowia lipolytica* [35].

NUOE and NUOF (a homologous of bovine 51 kDa) subunits have been purified and sequenced from subcomplex of NADH-CoQ reductase in *Rhodobacter capsulatus* [31] and *Escherichia coli* [36, 37]. In *Paracoccus denitrificans* studies, the NQO1 (also a homologous of bovine 51 kDa) has been identified as a NADH-binding catalytic subunit [38], and NQO2 subunit contains a single binuclear [2Fe-2S] cluster confirmed by electron paramagnetic resonance (EPR) analysis [32]. Similar to other species, NQO2 in *Paracoccus denitrificans* also assemble with NQO1 subunit to form a flavoprotein subcomplex in the proton-translocating NADH-quinone oxidoreductase (NDH-1) [39].

The NQO2 subunit contains seven cysteine residues. Among them, mutations in four conserved cysteine residues (C96, C101, C137 and C141) altered the UV-visible absorption spectra and EPR spectra [40]. This result indicated that these four cysteine residues are associated with the [2Fe-2S] cluster of *Paracoccus denitrificans* NQO2 subunit [40]. Human NDUFV2 also contains a binuclear [2Fe-2S] binding motif, Cys-(X)₄-Cys-(X)₃₅-Cys-(X)₃-Cys, which is very conserved from all orthologues [41].

The Nqo2 subunit in *Thermus thermophilus* HB-8 has similar optical and EPR properties compared to *Paracoccus denitrificans*. It also possesses higher protein stability to provide a great model to understand the structure-function relationship of this protein [33]. In the crystal structure data of the hydrophilic domain from *Thermus thermophilus* complex I, Nqo2 subunit is divided into two domains: one is N-terminal four helical bundles and the other is thioredoxin-like C-terminal domain. N-terminal domain interacts with Nqo1 and Nqo3 subunits, and the C-terminal domain

coordinates the binuclear cluster N1a [42]. Cluster N1a can accept electrons from FMN, but can not pass them to cluster N3, which is too far away from N1a. One hypothesis suggests that cluster N1a may act as an antioxidant to accept the excessive electrons to prevent the generation of ROS [26, 42].

The fungus *Neurospora crassa* is an eukaryotic organism which is frequently used as a model to study the structure and function of complex I [43]. In the *Neurospora crassa* studies, it was found that the lacking of nuo24 subunit would reduce the levels of 51 kDa subunit and affect the NADH:ferricyanide reductase activity, suggesting that the nuo24 subunit is essential for a proper assembly of 51 kDa subunit and complex I activity [34]. However, the nuo24 knock out strain had the normal oxygen consumption ability thus suggested that the nuo24 does not directly participate in the electron transferred process. In addition, it was found that the binding of [2Fe-2S] is essential for nuo24 assembly [34].

The amino acid sequence of mature 24 kDa in complex I has been purified and sequenced from bovine heart mitochondria [44]. Bovine complementary DNA (cDNA) sequences were used to hybridize human T cell cDNA library, the possible human precursor and mature sequences of 24 kDa subunit were identified. These results suggested that the N-terminal 1-32 amino acids of 24 kDa presequence may be the mitochondrial targeting sequence which contains an R-10 motif, xRx ↓ (F/L/I) xx(S/T/G)xxxx ↓, indicating a possible two-step processing by matrix proteinases including mitochondrial processing peptidase (MPP) and mitochondrial intermediate peptidase (MIP) [13, 45].

The deficiency of NDUFV2 subunit has been associated with some neurodegenerative diseases, including Parkinson disease [46], Alzheimer's disease

[47], Bipolar disorder and Schizophrenia [48, 49]. In the recent researches of early-onset hypertrophic cardiomyopathy and encephalopathy, the results showed that the patients with hypertrophic cardiomyopathy, trunk hypotonia and hyperlactatemia contained a homozygous mutation, a 4-bp deletion in intron 2 (IVS2+5_+8delGTAA) in the *NDUFV2*. This mutation altered the splicing donor site and caused the exon 2 losing in the mRNA of *NDUFV2*. This deletion decreased the amount of NDUFV2 protein and caused complex I deficiency in patients [50, 51]. Scientists have tried to simulate this exon 2 skipping mutation by deleting 17-32 residues of orthologous NUHM gene in the *Yarrowia lipolytica* model system. They originally expected that this deletion would affect the mitochondrial targeting ability of the predicted mitochondrial targeting sequence, NUHM 1-28, which contains the classic R-3 cleavage motif [52]. Surprisingly, the results showed that this mutant was indistinguishable from normal cells in activity, inhibitor sensitivity and EPR signals of complex I. Based on this result, they concluded that NUHM Δ 17-32 still possesses a functional mitochondrial targeting signal and the truncated NUHM does not hamper complex I assembly and function [35].

Some of the results from *Yarrowia lipolytica* were contradictory to those of the previously mentioned *Neurospora crassa* model. To clear out these discrepancies, we tried to focus on the functional role of NDUFV2 subunit in human cells in this study. We applied the RNA interference technology to suppress the NDUFV2 expression in human T-REx293 cells, and investigated the cell growth rate, oxygen consumption ability, complex I assembly and ROS levels in NDUFV2 knock-down cells.

In addition, we also wanted to investigate whether the IVS2+5_+8delGTAA mutation which caused the early-onset hypertrophic cardiomyopathy and encephalopathy disease could affect the assembly and function of NDUFV2 in human

cells. Furthermore, we also tried to identify the functional region and sequence features of the NDUFV2 MTS. It is expected that discoveries made in this study could help us to understand more about the association between gene mutations and diseases.



Materials and methods

1. Cell culture

T-REx-293 cells (Invitrogen, Eugene, USA) with tetracycline-regulated expression were cultured at 37 °C and 5 % CO₂ in Dulbeccos modified Eagle medium (DMEM) containing 10 % fetal bovine serum (FBS), 100 U/ml penicillin and 100 µg/ml streptomycin.

2. Protein sequence alignment

The following NDUFV2 protein sequences were obtained from the NCBI database: *Homo sapiens* NDUFV2 (NM_021074), *Bos taurus* 24 kDa (AAI02402), *Neurospora crassa* NUO-24 (X78083), *Yarrowia lipolytica* NUHM (AJ250338), *Paracoccus denitrificans* NQO2 (M74171), *Thermus aquaticus thermophilus* Nqo2 (U52917) and *Escherichia coli* APEC O1 NuoE (ABJ01673). Multiple sequence alignments of these NDUFV2 protein were generated by EMBL-EBI ClustalW2 ([http:// www. ebi. ac. uk/ Tools/ clustalw2/](http://www.ebi.ac.uk/Tools/clustalw2/)), and displayed by BOXSHADE server ([http:// www. ch. embnet. org/ software/ BOX_ form. html](http://www.ch.embnet.org/software/BOX_form.html)). The percentages of the sequence identity and similarity of these collected sequences were analyzed by FASTA.

3. Reduced expression of NDUFV2 by RNAi

The short hairpin (sh) RNA oligonucleotides of *NDUFV2* were designed according to the data base of National RNAi Core Facility (NRC) in Taiwan. The derived oligonucleotides: CCA GTT GGA AAG TAT CAC ATT CTC GAG AAT GTG ATA CTT TCC AAC TGG TTT TT were cloned into a pLKO.1-puro vector (Appendix 3) by *Age* I (NEB, Ipswich, USA) and *EcoR* I (NEB), and the resultant

plasmids were transfected into T-REx293 cells with Lipofectamine 2000 (Invitrogen). The stable clone cells were selected in a medium containing 2.5 $\mu\text{g/ml}$ puromycin.

4. Semi-quantitative reverse-transcription polymerase chain reaction (RT-PCR) analysis

The total cellular RNA of each cell lines was isolated by TRI reagent (molecular research center, Cincinnati, USA). Two micrograms of total RNA were converted to cDNA by reverse-transcriptase from ABI High Capacity cDNA RT kit (Applied biosystems, Lincoln, USA). Specific primers NDUFV2-F1: 5'-GAG ATA CTC CTG AGA ATA AC-3', NDUFV2-R3: 5'-GAG AAG CGT CCA CTC CTT GG-3', pLKO.1-F: 5'- GTT CTT GGG AGC AGC AGG -3' and pLKO.1-R: 5'-ATA GGC CCT CGG TGA AGG-3' were then designed and synthesized to detect the expression of *NDUFV2* gene and pLKO.1-puro plasmid. The glyceraldehyde 3-phosphate dehydrogenase (GAPDH-F1: 5'-GGG AAG CTT GTC ATC AAT GG-3' and GAPDH-R1: 5'-GCA TGG ACT GTG GTC ATG AG-3') gene was used as an internal control in RT-PCR analysis.

5. Western bolt analysis and antibodies

The stable clone cells were incubated with growth medium containing 0.5 $\mu\text{g/ml}$ tetracycline at 37 °C for 24 hr. Cells were collected by trypsinization and centrifuged at 4 °C at 1000 \times g for 5 min. The pellets were washed once and centrifuged at 4 °C at 1000 \times g for another 5 min. The pellets were then suspended with lysis buffer (0.15 M NaCl, 5 mM EDTA pH 8, 1 % Triton-X 100, 10 mM Tris-Cl, pH 7.4) for 20 min on ice and centrifuged at 4 °C at 14000 rpm for 10 min. After collecting the supernatants, the 4 \times dye was added and the resulted mixture was boiled for 5 min. Next, the proteins were separated by 10 % SDS-PAGE (sodium dodecyl sulphate

polyacrylamide gel electrophoresis) and transferred onto PVDF (polyvinylidene fluoride) at 350 mA current for 90 min. The membrane was then blocking with 5 % skin milk in phosphate-buffered saline (PBS) at room temperature for 90 min and incubated with diluted primary antibody at room temperature for 1 hr. After three times of PBS washing for 10 min each, the membrane was then incubated with proper secondary antibody at room temperature for 1 hr, and followed by several washes using PBS. Finally, the enhanced chemiluminescence (ECL) system (Perkin Elmer Life science, Massachusetts, USA) was used to detect the immunoreactive signals. The primary antibody detections were performed by using monoclonal mouse anti-c-myc antibody (Calbiochem, San Diego, USA), monoclonal mouse anti-EGFP antibody (SANTA CRUZ Biotechnology, Delaware, USA) and polyclonal rabbit anti-NDUFV2 antibody (SANTA CRUZ Biotechnology). The secondary detection was performed using goat anti-mouse or anti-rabbit IgG-HRP (Invitrogen).

6. Growth measurements

2×10^4 cells were seeded on 6-well plates in two different media. The glucose medium contained DMEM, 4.5 mg/ml glucose and 0.11 mg/ml pyruvate. The galactose medium lacked glucose and contained 0.9 mg/ml galactose and 0.5 mg/ml pyruvate. Both media contained 10 % FBS. Trypan blue dye was used to count the amount of cells for 8 consecutive days.

7. Oxygen consumption

The fresh medium was replaced 24 hr before the measurements. 5×10^6 cells were permeabilized by incubation with 1 ml respiration buffer (RB) (0.3 M mannitol, 10 mM KCl, 5 mM $MgCl_2$ and 10 mM K_2HPO_4 , pH 7.4) containing 60 μ g digitonin for 2 min at room temperature. Five milliliters of RB with 1 mg bovine serum albumin

(BSA) was then added to stop the reaction. The resultant cell suspension was centrifuged at $1000 \times g$ for 5 min. Finally, the pellets were suspended with 500 μ l RB containing 1 mg BSA and 1 mM ADP. Oxidation of the substrates, including 8 mM pyruvate and 0.2 mM malate, was measured by the Mitocell S200 micro respirometry system (Strathkelvin Instruments, Rowantree Avenue, North Lanarkshire). The reaction was stopped by adding 3 μ M rotenone [53].

8. Reactive oxygen species (ROS) assay

Cells were incubated with 20 μ M 5-(and-6)-carboxy-2',7'-dichlorodihydrofluorescein diacetate, carboxy-H₂DCFDA (Invitrogen), for 30 min and then were collected by trypsinization and centrifugation at $1000 \times g$ for 5 min. The pellets were washed once using 1 \times PBS and centrifuged at $1000 \times g$ for another 5 min. The pellets were then suspended with 1 \times PBS on ice. The ROS generation was determined using a FACScan flow cytometer (BD, Franklin Lakes, NJ USA). The data were processed by calculating the ratios of the mean fluorescence intensity.

9. Mitochondrial membrane potential (MMP) analysis

Cells were incubated with 200 nM lipophilic fluorophore tetramethylrhodamine methyl ester, TMRM (Invitrogen), for 20 min, and collected by trypsinization. 1×10^6 cells were washed once using 1 \times PBS and centrifuged at $1000 \times g$ for another 5 min. The pellets were then suspended with 1 \times PBS on ice. Samples were protected from light until the red fluorescence were determined by FACScan flow cytometer (BD).

10. High resolution clear native electrophoresis (hrCNE)

The hrCNE methodology was applied in this study to separate the mitochondrial respiratory complex I-V by using 6.5 % polyacrylamide gels. Seventy micrograms of mitochondrial proteins were loaded on each well in a gel with 8×10 cm dimensions.

The gel was run at 40 V for 30 min, and then at 80 V until the dye reached the end of the gel. Next, the gel was stained with coomassie blue for 1 hour and destained for 3 hours. The complex I was detected with complex I in gel staining buffer (5 mM Tris-HCl, pH 7.4; 0.1 mg/ml NADH; 2.5 mg/ml nitroterazolium blue, NTB) for 20 min at room temperature, and the reaction was stopped by fixing solution (50 % methanol; 10 % acetic acid) for 30 min at room temperature. Finally, the stained gel was stored in ddH₂O for later image analysis.

11. Constructs

(1) Construction of plasmids expressing full-length and truncated NDUFV2 proteins

The pcDNA4TM/TO/*myc*-His A vector (Invitrogen) (Appendix 4) was used as the expression plasmid, and *Eco*RI (NEB) and *Xho*I (NEB) were employed as restriction enzyme sites for cloning. The pcDNA4-NDUFV2 vector constructed in a previous study in Dr. Kao's laboratory was used as the template for its N-terminal deletion constructs (pcDNA4- Δ 1-18 NDUFV2, pcDNA4- Δ 1-32 NDUFV2 and pcDNA4- Δ 1-50 NDUFV2) and C-terminal deletion constructs (pcDNA4- Δ 183-249 NDUFV2 and pcDNA4- Δ 198-249 NDUFV2). The sequences of primers used are shown in Table 3-(2). Furthermore, the human pathogenic NDUFV2 mutant (pcDNA4- Δ 19-40 NDUFV2) in hypertrophic cardiomyopathy and encephalomyopathy was constructed. The primers used are shown in Table 3-(7).

(2) Construction of NDUFV2-EGFP

Various DNA fragments encoding different N-terminal proteins of NDUFV2 were designed and generated to fuse with *EGFP* gene in the pEGFP-N3

expression vector (Clontech Laboratories, Mountain view, CA, USA) (Appendix 5). The restriction enzyme sites used for this purpose are *XhoI* and *EcoRI* (NEB). The pcDNA4-NDUFV2 was used as the template to generate the various different N-terminal proteins of NDUFV2. These constructs were NDUFV2 full-length (pEGFP-N3 NDUFV2₁₋₂₄₉), pEGFP-N3 NDUFV2₁₋₃₂, pEGFP-N3 NDUFV2₁₋₂₂, pEGFP-N3 NDUFV2₁₋₂₁, pEGFP-N3 NDUFV2₁₋₂₀ and pEGFP-N3 NDUFV2₁₋₁₈. The sequences of primers used are shown in Table 3-(3).

(3) Construction of NDUFV2 missense mutants

The pcDNA4-NDUFV2 was used as the template for mutation of basic, hydroxylated and hydrophobic residues in first 1-32 amino acids of NDUFV2 using site-directed mutagenesis methodology. All of the used primers are shown in Table 3-(4, 5, 6).

12. Immunofluorescence staining

T-REx293 cells were seeded at approximately 60~70 % confluency in 24-well plates containing cover glasses and transfected by TransIT-LT1 transfection Reagent (Mirus, Madison, USA). Next, cells containing pcDNA4 expressing constructs were induced with the addition of 0.5 µg/ml tetracycline for 24 hr. After tetracycline induction, cells were incubated with growth medium containing 100 nM Mito Tracker Red (CMX-Ros; Molecular probe, Eugene, USA) for 30 min, and washed once in PBS. Then cells were permeated and fixed with acetone and methanol mixture (acetone: methanol = 3: 1 in volume proportion) for 5 min on ice. After fixation, cells were first incubated with growth medium at room temperature for 2 hr, and then with diluted monoclonal mouse anti-c-myc antibody (Calbiochem; 1:100 dilution) at room temperature for 1 hr. After 5 times of PBS washing, the cells were incubated with goat anti-mouse IgG-FITC (Invitrogen; 1:100 dilution) at room temperature for another 1

hr, and washed again by PBS. Finally, the cover glass was mounted by VECTASHIELD Mounting Medium (Vector Laboratories, Burlingame, USA). Fluorescence was visualized by LSM510 confocal microscope (ZEISS; Welwyn Garden City; Germany).



Results

A. The functional studies of NDUFV2

1. Reduced expression of NDUFV2 by RNAi.

In order to understand the function of NDUFV2 in human cell, RNA interference (RNAi) technology was used to knock down the expression of *NDUFV2* in T-REx293 cells, and two independent cell lines, 1F4 and 1F6, expressing pLKO.1-puro plasmids were established in this study (Figure 2-A). The results from the quantification of the semi-quantitative RT-PCR and real-time PCR indicated that the NDUFV2 mRNA levels were decreased by 85.1 % and 87.6 % respectively in 1F4 and 1F6 cells (Figure 2-A, B). As for the results of western blotting detection with rabbit polyclonal anti-NDUFV2 antibody, the protein expression levels of NDUFV2 were decreased by 53.4 % and 33.9 % in these two knock-down cell lines (Figure 2-C).

2. Suppression of NDUFV2 expression in T-REx293 cells led to a slow grow rate in galactose containing medium.

Mammalian cells rely on glycolysis and mitochondrial oxidative phosphorylation for ATP production. Using galactose in the medium as the energy source instead of glucose will force cells to rely on mitochondrial oxidative phosphorylation pathway for their energy requirement. Using this strategy the condition of mitochondria in cells could be evaluated. In glucose containing medium, the 1F4 and 1F6 cells grew as well as the T-REx293 cells (Figure 3-A), but failed to grow and finally died in galactose containing medium (Figure 3-B). These results indicated that the suppressed NDUFV2 cell lines were unable to obtain enough energy from mitochondria thus caused a slow grow rate.

3. The amount of oxygen consumption was decreased in NDUFV2 knock-down cells.

To investigate the oxidative phosphorylation capacity of cells with NDUFV2 suppression in galactose containing medium, the respiratory properties of 1F4, 1F6 and T-REx293 cells were measured. Pyruvate and malate were used as the complex I substrate and added to the digitonin-permeabilized cells for oxygen consumption measurement. The results showed that, compared with the result from T-REx293 cells, the oxygen consumption of 1F4 and 1F6 was decreased by 37.5-61.5 % (Figure 4-B). It indicated that the NDUFV2 is essential for the cell respiratory capacity. When complex I inhibitor, rotenone, was added to the reaction mixture, the electron transfer was stopped and the oxygen consumption rates of cells were suppressed (Figure 4-A).

4. The suppression of NDUFV2 expression in T-REx293 cells decreased the MMP.

The MMP of cells were labeled with TMRM, MMP indicator, and determined by a FACScan flow cytometer. As shown in Figure 5, the MMP decreased by 46.21 % and 8.90 % in 1F4 and 1F6 cell lines comparing with the result from T-REx293 cells. These results indicated that the suppression of NDUFV2 expression compromised the maintaining of electrochemical proton gradient which is essential for energy production in OXPHOS.

5. The suppression of NDUFV2 expression in T-REx293 cells increased the generation of ROS.

In previous studies, scientists suggested that the N1a cluster may act as an antioxidant to accept the excessive electrons to prevent the generation of ROS [26, 42]. To confirm this viewpoint, carboxy-H₂DCFDA, a membrane-permeable fluorescent dye, was used to detect the levels of intracellular H₂O₂ in the NDUFV2

knock-down cell lines. The fluorescence intensity was determined by a FACScan flow cytometer. The results showed that the generation of H₂O₂ increased by 26.67 % and 8.85 % in 1F4 and 1F6 cell lines comparing with the result from T-REx293 cells (Figure 6). It revealed that suppression of *NDUFV2* expression would affect the amount of ROS generation in cells.

6. NDUFV2 dose not affect complex I assembly.

In order to understand whether NDUFV2 could affect the complex I assembly, high resolution clear native electrophoresis (hrCNE) was applied to separate and characterize mitochondrial respiratory complexes, followed by in-gel catalytic activity assay to label the position of complex I. The results showed that the complex I assembled patterns of NDUFV2 knock-down cell lines did not show significant differences from the T-REx293 cell line (Figure 7), this finding suggested that NDUFV2 subunit in the T-REx293 cells may not be directly involved in complex I assembly.

B. Characterization of the mitochondrial targeting signal in NDUFV2

1. The MTS of NDUFV2 was located at the N-terminus of the protein and its cleavage site was located around amino acid residue 32.

The protein sequence alignment of NDUFV2 revealed that eukaryotic species have one non-conserved fragment located at the N-terminus of NDUFV2 (Figure 1). It was predicted that the fist 1-32 amino acids of NDUFV2 may be the mitochondria targeting sequence (MTS) of this protein [45]. To test this prediction, various N-terminal and C-terminal deletion constructs were generated to identify the location

and orientation of MTS in NDUFV2 (Figure 8-A). Using immunofluorescent staining methodology, mouse anti-c-myc antibody was applied to detect the expressed proteins, and the Mito Tracker Red dye was used to mark the mitochondria. The results showed that pcDNA4-NDUFV2 and its C-terminal deletion constructs (pcDNA4- Δ 183-249 NDUFV2 and pcDNA4- Δ 198-249 NDUFV2) could colocalize with mitochondria, but its N-terminal deletion constructs (pcDNA4- Δ 1-18 NDUFV2, pcDNA4- Δ 1-32 NDUFV2 and pcDNA4- Δ 1-50 NDUFV2) could not (Figure 8-B). These results confirmed the prediction from protein sequence alignment that the MTS of NDUFV2 was located at the N-terminus of the protein.

In previous studies, the NDUFV2 contains an R-10 motif, xRx↓ (F/L/I)xx (S/T/G)xxxx↓, indicating a possible two-step processing by matrix proteinases [13, 45]. In order to understand whether NDUFV2 was cleaved by matrix proteinases and identify the cleavage site of this protein, various N-terminal deletions of NDUFV2 carrying C-terminal myc tag were expressed in T-REx293 and detected by western blotting with mouse anti-c-myc antibody. The sizes of these N-terminal deletion proteins, pcDNA4- Δ 1-18 NDUFV2, pcDNA4- Δ 1-32 NDUFV2 and pcDNA4- Δ 1-50 NDUFV2, were compared with full-length NDUFV2 construct (Figure 9). The results showed that the migration of the pcDNA4- Δ 1-18 NDUFV2 mutant was larger and the pcDNA4- Δ 1-50 NDUFV2 mutant was smaller than the processed NDUFV2, but just the truncated protein lacking first 32 amino acids had a similar size with processed NDUFV2. These data revealed that the first 18 amino acids of NDUFV2 are essential for mitochondrial targeting, so this truncated protein would not be processed thus caused its larger size. In contrast, the deletion mutant lacking the first 50 amino acids was shorter than the correctly processed NDUFV2

and indicated that the cleavage site must be less than residue 50. Finally, the cleavage site was confirmed to be located around residue 32 of NDUFV2 precursor protein because the corrected processed NDUFV2 had the same migration location with the pcDNA4- Δ 1-32 NDUFV2 mutant.

2. The N-terminal sequence of NDUFV2 including amino acids 1-22 could carry the EGFP to mitochondria.

Next, a series of N-terminal peptides were constructed and fused with EGFP to identify the range of functional MTS (Figure 10-A). These results showed that just the first 22 residues of NDUFV2 were enough to carry most of the EGFP into mitochondria successfully. Although N-terminal sequence 1-21 or 1-20 of NDUFV2 constructs was also able to direct EGFP to mitochondria, the efficiency was much lower in these constructs. When the first 1-18 amino acid residues were used as the MTS, no mitochondria targeting abilities of this hybrid protein was found (Figure 10-C).

Moreover, when the N-terminal 1-22 residues was moved to the C-terminus of EGFP, the mitochondrial targeting capability of this just identified MTS was lost (Figure 11-B). These results suggested that the MTS of NDUFV2 is directional. Interestingly, when the N-terminal 5-22 residues were used to carry EGFP, the resultant hybrid protein could not be transported to mitochondria successfully. This result indicated that the completed 1-22 residues are necessary for mitochondria targeting.

3. Both basic and hydrophobic residues in MTS were very important for mitochondrial targeting of NDUFV2, but the hydroxylated residues were not.

As reviewed in the introduction, most mitochondrial matrix proteins contain a amino-terminal presequence which includes a positively charged amphipathic α -helix

that is rich in basic, hydrophobic and hydroxylated residues, but lacks acidic amino acids [11, 12]. To test whether the aforementioned features are also applicable to the MTS of NDUFV2, PSIPRED server ([http:// bioinf. cs. ucl. ac. uk/ psipred/ psiform. html](http://bioinf.cs.ucl.ac.uk/psipred/psiform.html)) was used to predict the secondary structure of NDUFV2 (Figure 12-A), and Helical Wheel Projections program ([http:// rzlab. ucr. edu/ scripts/ wheel/ wheel. cgi](http://rzlab.ucr.edu/scripts/wheel/wheel.cgi)) was applied to construct the α -helical wheel model for N-terminus of NDUFV2 (Figure 12-B). It is clear that the N-terminus of NDUFV2 contains a typical positively charged amphipathic α -helix structure. We then used the site-directed mutagenesis methodology to identify the role of these three kinds of residues in NDUFV2 MTS. First, we mutated all hydroxylated residues in NDUFV2 MTS and found that the mitochondrial targeting ability of this protein was not affected (Figure 13). The N-terminal 1-32 amino acids of NDUFV2 contain eight basic residues. The mutations in each individual basic residue did not affect the mitochondrial targeting function (data not show). However, when all of the eight basic residues were mutated, the ability of mitochondrial targeting would be destroyed (Figure 14). Finally, we found that the mitochondrial targeting ability of NDUFV2 MTS was affected by mutating more than five hydrophobic residues in NDUFV2 N-terminus (Figure 15). All of these results indicated that the basic and hydrophobic residues were very important for the MTS of NDUFV2, but the hydroxylated residues were not.

4. Establishing the human disease mechanism of the early-onset hypertrophic cardiomyopathy and encephalopathy.

The patients of early-onset hypertrophic cardiomyopathy and encephalopathy contain a homozygous mutation, a 4-bp deletion in intron 2 (IVS2+5_+8delGTAA), in *NDUFV2*. This mutation alters the splicing donor site to cause the exon 2 losing and encodes a shortened NDUFV2 that lacks 19-40 residues [51] (Figure 16-A). In

Yarrowia lipolytica model studies, amino acids 17-32 from the NUHM have been deleted to mimic this disease. However, it was found that the resultant mutant was indistinguishable from the normal protein in activity, inhibitor sensitivity and EPR signals of complex I [35] .

To clarify the association of this mutation with the disease, human T-REx293 cells were used as the modeling system in this study. The result showed that the human pathogenic NDUFV2 mutant, the amino acids 19-40 deletion of NDUFV2, was unable to target to mitochondria (Figure 16-B). In addition, it was found that the N-terminal secondary structure of NDUFV2 mutant was destroyed completely and changed from α to β form (Figure 16-C).

According to these results, it is clear that the NDUFV2 mutant (Δ 19-40) could not be imported to mitochondria successfully. This deletion causes NDUFV2 to just have its first 18 residues of MTS remained thus loses its mitochondrial targeting ability. This conclusion was also confirmed by the mitochondrial targeting data from pEGFP-N3-NDUFV2₁₋₁₈-EGFP constructs (Figure 10-C). When functional NDUFV2 could not be imported to mitochondria by the defected MTS, complex I will lose its function in the energy transduction pathway.

Discussion

The functional studies of NDUFV2

According to the experiments results presented in this study suppression of NDUFV2 expression in human cells could lead to a slow growth rate in galactose containing medium, a decreased oxygen consumption rate, a decreased MMP and increased ROS generation, but the NDUFV2 is not essential for complex I assembly and NADH oxidation ability based on the data from hrCNE and in gel catalytic activity assay. Summarizing these observations provided evidences that NDUFV2 had an essential role for energy production in the OXPHOS of cells but may not be in a critical position to affect complex I assembly. However, in the *Neurospora crassa* studies, scientists have found that lacking of nuo24 subunit would reduce the levels of 51 kDa subunit and affect the NADH:ferricyanide reductase activity, but the cells still had the normal oxygen consumption ability [34]. In the *Neurospora crassa* model system, these organisms contain several different metabolic pathways from mammalian cells which may cause the discrepancy shown here. It has been demonstrated that when some of the fungi lack the NADH oxidation ability of complex I because of mutations, they can use the alternative NADH dehydrogenases pathway to compensate these defects [54, 55]. Therefore, using human cell model as shown in this study could avoid the possible divergence derived from different metabolic pathways existing among different species and be closer to the real situation in human bodies.

In this report, because of the lack of applicable antibody, we did not check the assembly levels of NDUFV1 (51 kDa), a NADH-binding and catalytic subunit, in

NDUFV2 suppressed cell lines. However, the results of complex I in gel assay suggested that the complex I NADH oxidation abilities of NDUFV2 suppressed cells do not have significant differences from those of normal cells.

Previous structural studies implied that the cluster N1a may act as an antioxidant to accept the excessive electrons to prevent the generation of ROS [26, 42]. To respond to this hypothesis, we found that the level of H₂O₂ generation increased in NDUFV2 suppressed cell lines. In the future, we plan to conduct similar experiments under oxidative stress conditions to see if this H₂O₂ level increasing is even more significant. In addition, we also want to test whether the NDUFV2 overexpression cells have the capabilities of preventing or reducing the generation of ROS under oxidative stress situation. Furthermore, we will also detect the other ROS like superoxide (O²⁻) using hydroethidine (HE) using similar strategies.

The studies of mitochondrial targeting signals of NDUFV2

The N-terminal 1-32 amino acids of bovine 24 kDa presequence have been suggested to contain the mitochondrial targeting sequence [44, 45]. In this report, we identified that the cleavage site of human NDUFV2 was located around amino acid residue 32 and the functional mitochondrial targeting region was located at the N-terminal amino acids 1- 22. This MTS was directional and contained classical positively charged amphipathic α -helix structure. We also found that the basic and hydrophobic residues in this region were very important for the mitochondrial targeting function of MTS in NDUFV2, but the hydroxylated residues were not.

Data from clinical researches indicated that the patients suffering from early-onset hypertrophic cardiomyopathy and encephalopathy disease frequently contain a 4-bp deletion in intron 2 (IVS2+5_+8delGTAA) of the *NDUFV2*. This

mutation alters the splicing donor site to cause the exon 2 losing and encode a shortened NDUFV2 that lacks 19-40 residues [50, 51]. In studies using *Yarrowia lipolytica* as the model, it was found that the truncated proteins caused by this exon 2 skipping mutation because of deleting 17-32 residues of orthologous NUHM gene is indistinguishable from normal proteins in activity, inhibitor sensitivity and EPR signals of complex I [35]. The results from our established human investigating model indicated that the partial deletion of MTS in pathogenic NDUFV2 destroyed the mitochondrial import capability of this protein. When just the first 1-18 residues of NDUFV2 were remained in the MTS, no mitochondrial targeting was observed. Though there is highly conservation between human NDUFV2 subunit and *Yarrowia lipolytica* NUHM with 62.7% identity and 82.5% similarity (Table 1), the functional MTS of NUHM have not been experimentally identified. We hypothesize that losing 17-32 amino acid residues in the NUHM does not destroy the functional MTS region of this protein so that this mutant protein could still be transported to mitochondria and retain its normal activities in complex I. In order to support this hypothesis, we used the MitoProt II -v1.101 Server (<http://hg2.elmholtz-uenchen.de/hg/itoprot.tml>) to predict the possible MTS of NUHM and the result showed that it is located at the first 16 amino acids. In addition, we also used the Predotar v. 1.03 Server (<http://urgi.versailles.inra.fr/predotar/predotar.html>) to predict the location of MTS in the mutant NUHM, and found that the Δ 17-32 NUHM mutant still has a high degree of mitochondrial targeting score similar to that of the intact NUHM (Table 2). Moreover, the N-terminal region of Δ 17-32 NUHM mutant did not lose its amphipathic α -helix pattern predicted by Helical Wheel Projections program (Figure 17). The real situation in *Yarrowia lipolytica* on this issue requires further experiments to confirm.

Some disease mutations caused to affect protein localization are called

mislocalization mutations. For example, the short stature homeobox gene (SHOX) is a cell-type-specific transcriptional activator and the missense mutation R173C (C517T) of this gene is unable to enter the nucleus thus causes Leri-Well dyschondrosteosis (LWD) and Langer mesomelic dysplasia (LD) [56]. Another example is human tafazzin (Taz1p), a membrane-associated mitochondrial acyltransferases. Some mutations in this protein alter protein targeting and assembly within mitochondria thus cause Barth syndrome (BTHS) [57]. These examples support our argument that the mislocalization mutations of NDUFV2 could be associated with early-onset hypertrophic cardiomyopathy and encephalopathy disease.



Tables

Table 1

Sequence identity and similarity (%) of *H. sapiens* NDUFV2 to subunits from various organisms

Species	Identity(%)	Similarity(%)
<i>Bos taurus</i>	96.8	99.6
<i>Neurospora crassa</i>	62.7	84.4
<i>Yarrowia lipolytica</i>	58.0	82.5
<i>Paracoccus denitrificans</i>	43.8	74.7
<i>Thermus aquaticus thermophilus</i>	40.0	74.7
<i>Escherichia coli</i>	35.2	69.7

**Table 2.**

The Predotar v. 1.03 Server predicts the location of these proteins.

	Mitochondria	ER	Elsewhere
NUHM	0.95	0.01	0.08
\triangle 17-32 NUHM	0.94	0.01	0.06
NDUFV2	0.85	0.01	0.15
\triangle 19-40 NDUFV2	0.46	0.01	0.54
\triangle 23-40 NDUFV2	0.64	0.01	0.36

Table 3.

Sequences of the primers used in this study:

(1) For RT-PCR

NDUFV2	24K-F1	GAGATACTCCTGAGAATAAC
	24K-R3	GAGAAGCGTCCACTCCTTGG
GAPDH	GAPDH-F1	GGGAAGCTTGTCATCAATGG
	GAPDH-R1	GCATGGACTGTGGTCATGAG
pLKO.1-puro-plasmid	pLKO1-puro-F	GTTCTTGGGAGCAGCAGG
	pLKO1-puro-R	ATAGGCCCTCGGTGAAGG

(2) For pcDNA4-Del NDUFV2 MTS

delNDUFV2 1-32	dMTS 24 kDa-F1	CGAATTCATGGGAGCTGGAGGAGCTTTA
delNDUFV2 1-20	dMTS 24 kDa-F2	CGAATTCATGCATGTAAGGAATTTGCAT
delNDUFV2 1-18	dMTS 24 kDa-F3	CGAATTCATGGGAAGACATGTAAGGAAT
delNDUFV2 1-40	dMTS 24 kDa-F4	CGAATTCATGCACAGAGATACTCCTGAG
delNDUFV2 1-50	dMTS 24 kDa-F5	CGAATTCATGACTCCATTTGATTTACAC
	dMTS 24 kDa-R1	GCTCGAGAAGGCCTGCTTGTACACC

(3) For pEGFP-N3-NDUFV2

	24K-MTS- N3-1F	CCTCGAGATGTTCTTCTCCGCGGCG
	24K-MTS-N3-2F	CCTCGAGATGCGGGCCCCGGGCGGCTGGC
NDUFV2-1~18 (1F1R)	24K-MTS- N3-1R	CGAATTCGCCCAGTGGGCGGTGAGGCC
NDUFV2-1~40 (1F2R)	24K-MTS- N3-2R	CGAATTCGCCACAAATAAAGCTCCTCC
NDUFV2-1~32 (1F3R)	24K-MTS- N3-3R	CGAATTCGCATTTTGCATAGCTGTCTT
NDUFV2-1~249 (1F4R)	24K-MTS- N3-4R	CGAATTCGCAAGGCCTGCTTGTACACC
NDUFV2-1~27 (1F5R)	24K-MTS- N3-5R	CGAATTCGCCTTATGCAAATTCCTTAC
NDUFV2-1~23 (1F6R)	24K-MTS- N3-6R	CGAATTCGCCCTTACATGTCTTCCCCAG
NDUFV2-1~22 (1F8R)	24K-MTS- N3-8R	CGAATTCGCTACATGTCTTCCCCAGTG
NDUFV2-1~20 (1F9R)	24K-MTS- N3-9R	CGAATTCGCTCTTCCCCAGTGGGCGGTG
NDUFV2-1~21 (1F10R)	24K-MTS- N3-10R	CGAATTCGCATGTCTTCCCCAGTGGGC
NDUFV2-8~22 (2F8R)	24K-MTS- N3-8R	CGAATTCGCTACATGTCTTCCCCAGTG

(4) For pcDNA4-Hydroxylated residues mutation-NDUFV2

T15A	24 kDa MTS T15A-F	GGCGGCTGGCCTCGCAGCCCCTGGGGAAG
	24 kDa MTS T15A-R	CTTCCCCAGTGGGCTGCGAGGCCAGCCGCC
S4G	24 kDa-MTS-S4G-F	CCGCCATGTTCTTCGGAGCGGCGCTCCGGG
	24 kDa-MTS-S4G-R	CCCGGAGCGCCGCTCCGAAGAACATGGCGG
T28A	24 kDa-MTS-T28A-F	GGAATTTGCATAAGGCAGTTATGCAAAATG
	24 kDa-MTS-T28A-R	CATTTTGCATAACTGCCTTATGCAAATTCC

(5) For pcDNA4-Basic residues mutation-NDUFV2

R8G	24 kDa MTS CCG21,22,24AGT(R8G)-F	TCTCCGCGGCGCTAGGTGCCCCGGGCGGCTG
	24 kDa MTS CCG21,22,24AGT-(R8G)R	CAGCCGCCCCGGGCACCTAGCGCCGCGGAGA
R10A+H17A+ R8G	24 kDa-MTS-R8G-2F	TCTCCGCGGCGCTAGGTGCCGCGGCGGCTG
	24 kDa-MTS-R8G-2R	CAGCCGCGCGGCGCACCTAGCGCCGCGGAGA
R10A	24 kDa MTS CG28,29GC(R10A)-F	CGGCGCTCCGGGCGCGGCGGCTGGCCTCA
	24 kDa MTS CG28,29GC(R10A)-R	TGAGGCCAGCCGCCGCGGCCCGGAGCGCCG
R8G+H17A+ R10A	24 kDa-MTS-R10A-F2	CGGCGCTAGGTGCCGCGGCGGCTGGCCTCA
	24 kDa-MTS-R10A-R2	TGAGGCCAGCCGCCGCGGCACCTAGCGCCG
H17A	24 kDa MTS CG49,50GC(H17A)-F	CTGGCCTCACCGCCGCCTGGGGAAGACATG
	24 kDa MTS CG49,50GC(H17A)-R	CATGTCTTCCCCAGGCGGCGGTGAGGCCAG
R8G+R10A+H17A+ H21A	24 kDa-MTS-H21A-F	CCGCCTGGGGAAGAGCTGTAAGGAATTTGC
	24 kDa-MTS-H21A-R	GCAAATTCCTTACAGCTCTTCCCCAGGCGG
R8G+R10A+H17A+H21A+ R20A	24 kDa-MTS-R20A-F	CGCCGCCTGGGGAGCAGCTGTAAGGAATT
	24 kDa-MTS-R20A-R	AATTCCTTACAGCTGCTCCCCAGGCGGCG
R8G+R10A+H17A+H21A+R20A+ R23A	24 kDa-MTS-R23A-F	GGGAGCAGCTGTAGCGAATTTGCATAAG
	24 kDa-MTS-R23A-R	CTTATGCAAATTCGCTACAGCTGCTCCC
R8G+R10A+H17A+H21A+R20A+R23A+ H26A	24 kDa-H26A-F	CTGTAGCGAATTTGGCTAAGACAGTTATG
	24 kDa-H26A-R	CATAACTGTCTTAGCCAAATTCGCTACAG
R8G+R10A+H17A+H21A+R20A+R23A+H26A+ K27A	24 kDa-K27A-F	GTAGCGAATTTGGCTGCGACAGTTATGCAA
	24 kDa-K27A-R	TTGCATAACTGTCGCAGCCAAATTCGCTAC

(6) For pcDNA4-Hydrophobic residues mutation-NDUFV2

L7Q	24 kDa-MTS-L7Q-F	CTTCTCCGCGGCGCAACGGGCCCCGGGCGGC
	24 kDa-MTS-L7Q-R	GCCGCCCCGGGCCCCGTTGCGCCGCGGAGAAG
L14Q	24 kDa-MTS-L14Q-F	CCGGGCGGCTGGCCAAACCGCCCACTGGG
	24 kDa-MTS-L14Q-R	CCCAGTGGGCGGTTTGGCCAGCCGCCCCGG
L25Q	24 kDa-MTS-L25Q-F	GACATGTAAGGAATCAGCATAAGACAGTTA
	24 kDa-MTS-L25Q-R	TAAGTGTCTTATGCTGATTCCTTACATGTC
V22G	24 kDa-V22G-F	CTGGGGAAGACATGGAAGGAATCAGCATA
	24 kDa-V22G-R	TATGCTGATTCCTTCCATGTCTTCCCCAG
V29G	24 kDa-V29G-F	CAGCATAAGACAGGTATGCAAAATGGAG
	24 kDa-V29G-R	CTCCATTTTGCATACCTGTCTTATGCTG
L7,14,25Q+ V22G	24 kDa-V22G-F2	CTGGGGAAGACATGGAAGGAATTTGCATA
	24 kDa-V22G-R2	TATGCAAATTCCTTCCATGTCTTCCCCAG
L7,14,25Q+V22, 29G	24 kDa-V29G-F2	TTGCATAAGACAGGTATGCAAAATGGAG
	24 kDa-V29G-R2	CTCCATTTTGCATACCTGTCTTATGCAA
F2Y	24 kDa-F2Y-F	GAATTCCCEGCCATGTACTTCTCCGCGGCG
	24 kDa-F2Y-R	CGCCGCGGAGAAGTACATGGCGGGGAATTC
F3Y	24 kDa-F3Y-F2	CCCCGCCATGTTCTACTCCGCGGCGCTCCG
	24 kDa-F3Y-R2	CGGAGCGCCGCGGAGTAGAACATGGCGGGG
W18Y	24 kDa-W18Y-F2	CTCACC GCCCACTATGGAAGACATGTAAG
	24 kDa-W18Y-R2	CTTACATGTCTTCCATAGTGGGCGGTGAG
L7,14,25Q+V22,29G+ W18Y	24 kDa-W18Y-F	CAAACCGCCCACTATGGAAGACATGGAAG

	24 kDa-W18Y-R	CTTCCATGTCTTCCATAGTGGGCGGTTTG
L7,14,25Q+V22,29G+W18Y+F3Y	24 kDa-F3Y-F	CCCCGCCATGTTCTACTCCGCGGCGCAAC
	24 kDa-F3Y-R	GTTGCGCCGCGGAGTAGAACATGGCGGGG

(7) For pcDNA4-Del (19-40) NDUFV2

dE2-Not1-R	GCGGCCCGCACCAAGTGGGCGGTGAGGCC
dE2-Not1-F	GCGGCCCGCCACAGAGATACTCCTGAG
ddE2-F	GCTGGCCTCACCGCCCACTGGCACAGAGATACTCCTGAGAATAAC
ddE2-R	GTTATTCTCAGGAGTATCTCTGTGCCAGTGGGCGGTGAGGCCAGC
24 kDa-ddE2-m-F	GGGCCAAGGAGTGGACGCTTCTCTTGTG
24 kDa-ddE2-m-R	CACAAGAGAAGCGTCCACTCCTTGGCCC

(8) For pcDNA4-NDUFV2-PM

pCDNA4-24 kDa-mutation-F	ATCGAAAGCCAGTTGGGAAATACCACATTCAGGTCTGC
pCDNA4-24 kDa-mutation-R	GCAGACCTGAATGTGGTATTTCCCAACTGGCTTTCGAT

Figures

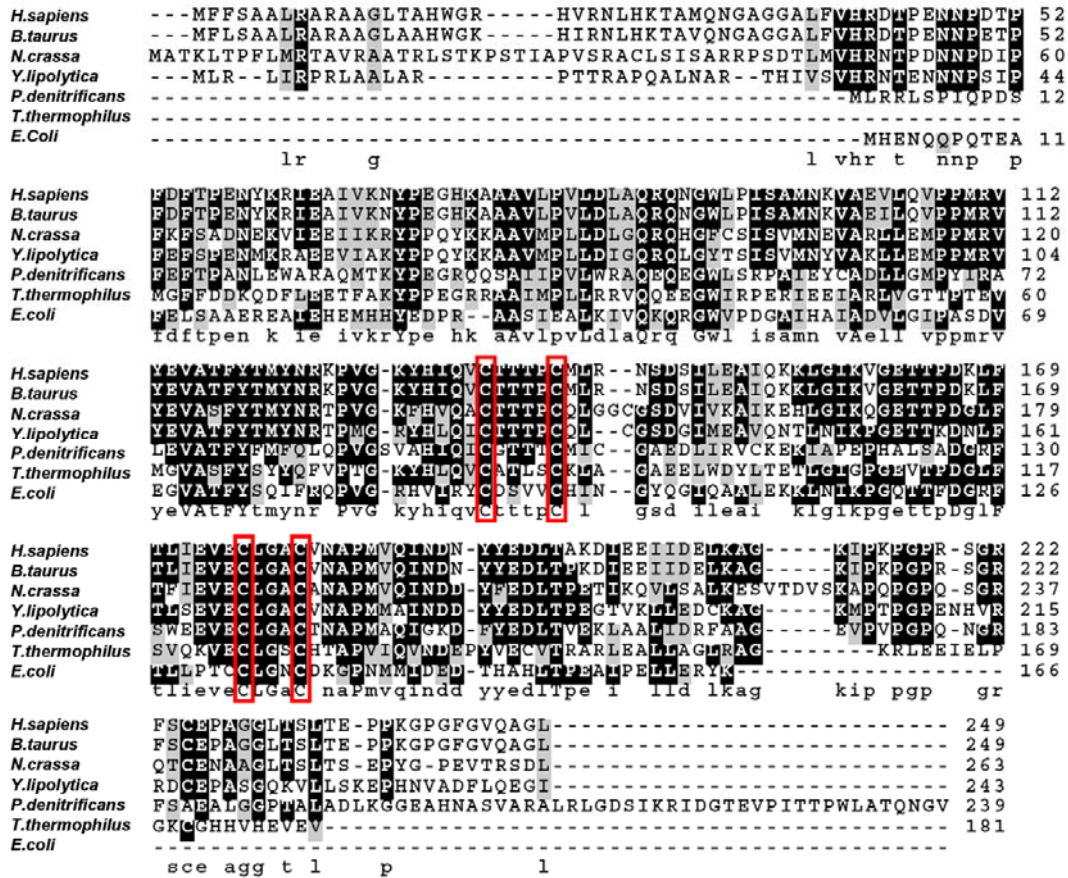
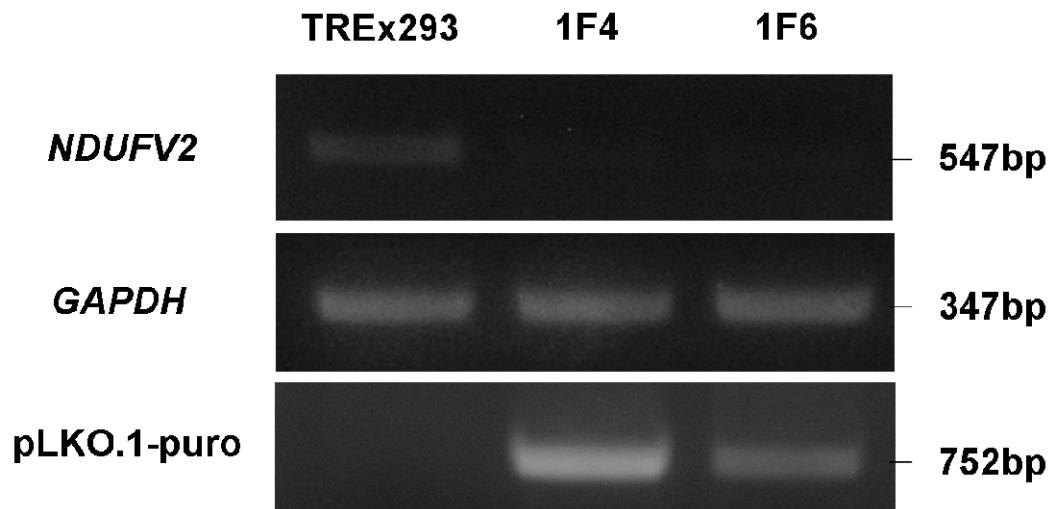
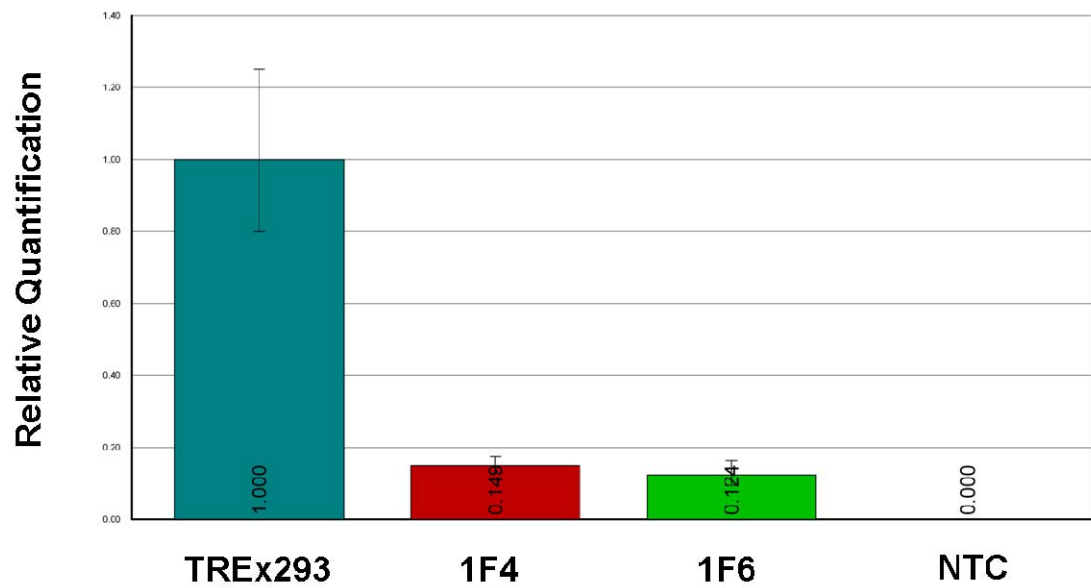


Figure 1. Multiple sequence alignment of NDUFV2 proteins from different species. Sequence alignment was generated by EMBL-EBI Clustal W2 ([http:// www. ebi. ac. uk/ Tools/ clustalw2/](http://www.ebi.ac.uk/Tools/clustalw2/)) and displayed by BOXSHADE server ([http:// www. ch. embnet. org/ software/ BOX_ form. html](http://www.ch.embnet.org/software/BOX_form.html)). Red boxes are cysteine residues of [2Fe-2S] cluster motif: Cys(X)₄-Cys(X)₃₅-Cys(X)₃-Cys. The abbreviation used are: *H. sapiens*, *Homo sapiens* NDUFV2 (NM_021074); *B. taurus*, *Bos taurus* 24 kDa (AAI02402); *N. crassa*, *Neurospora crassa* NUO-24 (X78083); *Y. lipolytica*, *Yarrowia lipolytica* NUHM (AJ250338); *P. denitrificans*, *Paracoccus denitrificans* NQO2 (M74171); *T. thermophilus*, *Thermus aquaticus thermophilus* Nqo2 (U52917) and *E. coli*, *Escherichia coli* APEC O1 NuoE (ABJ01673).

A



B



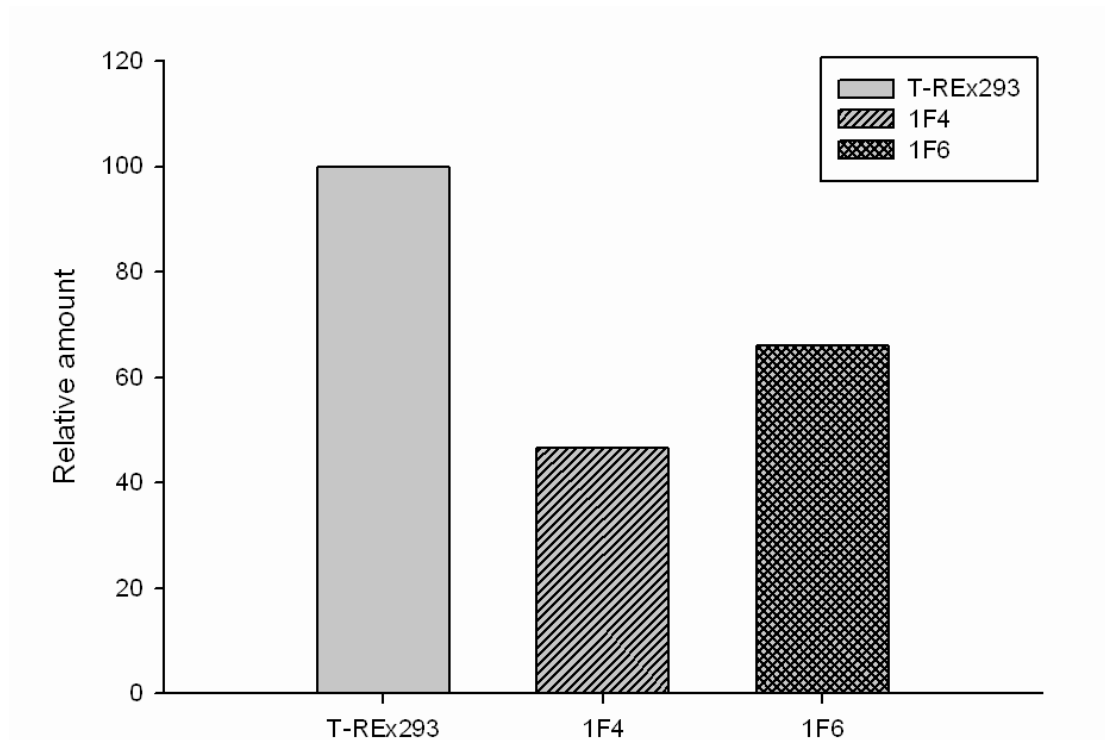
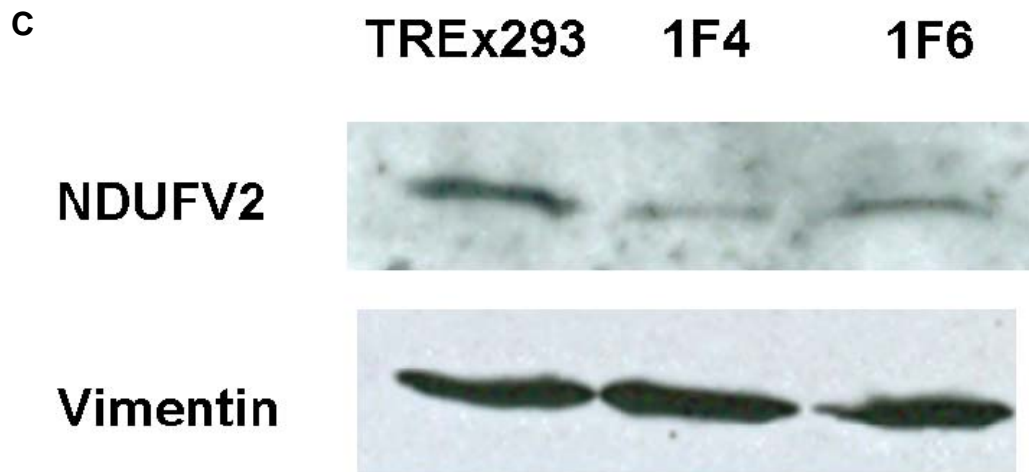


Figure 2. The RNAi effect on NDUFV2 mRNA and protein level

(A) RT-PCR was used to detect the *NDUFV2* expression levels in TREx293, 1F4 and 1F6 cells. (B) Quantification of the relative amounts of the expressed *NDUFV2* was determined by Applied Biosystems 7500 real-time PCR system, and normalized by the expression of GAPDH. (C) The *NDUFV2* protein expression levels in TREx293, 1F4 and 1F6 cells were detected by western blotting and quantified using ImageJ densitometry. Values were normalized by the intensity of vimentin. Cell lysates were run on 10% SDS-PAGE, and blotted with rabbit polyclonal anti-NDUFV2 antibody.

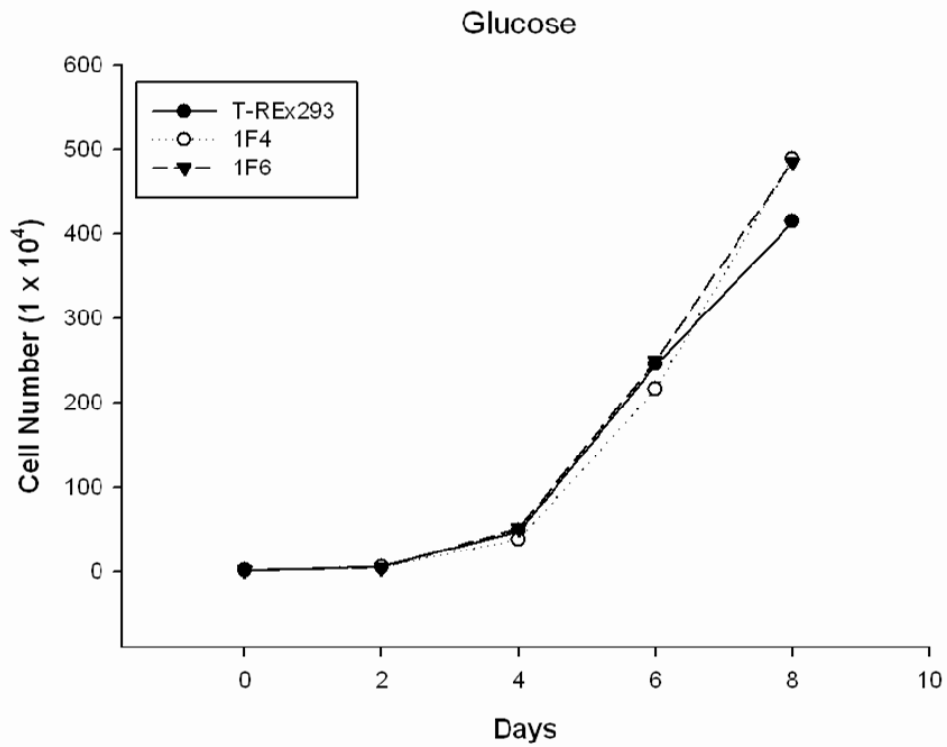
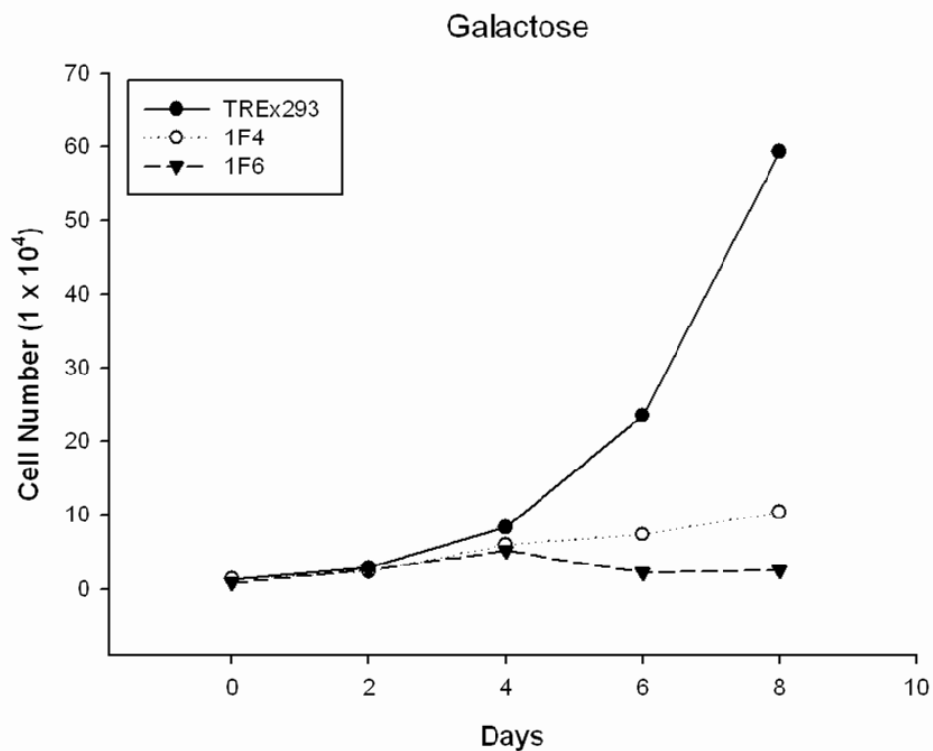
A**B**

Figure 3. The growth rate of T-REx293 and NDUFV2 knock down 1F4 and 1F6 cell lines were measured in glucose (A) and galactose (B) containing medium. Cells were seeded at 2×10^4 per well at first day 0 and counted for 8 days.

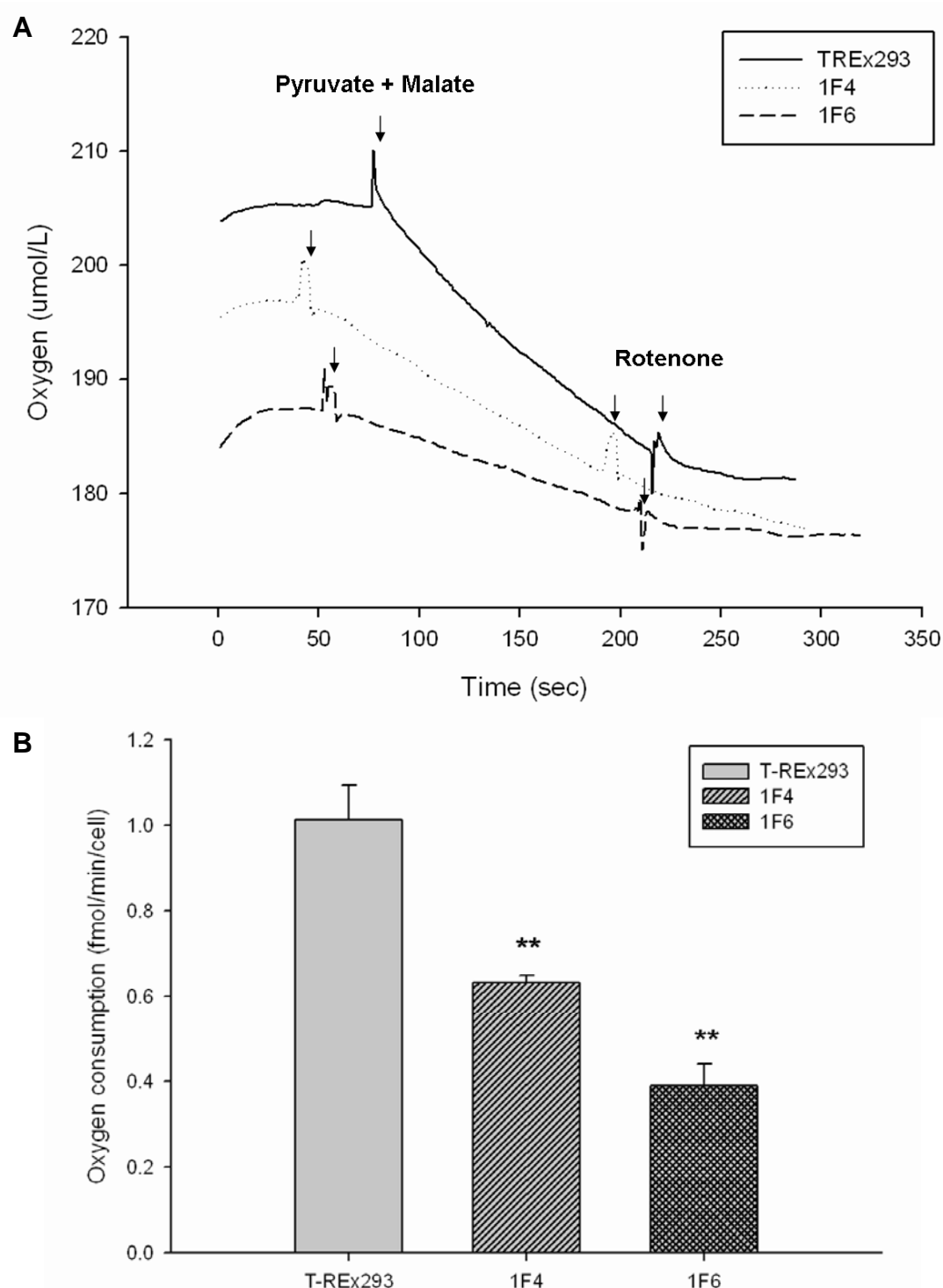


Figure 4. Cellular oxygen consumption assay of T-REx293, 1F4 and 1F6 cells was measured by Mitocell S200 micro respirometry system. (A) The illustration of oxygen consumption experiment by digitonin-permeabilized cells. (B) The percentages of cellular oxygen consumption rates (O_2 fmol/ min/ cell) in T-REx293, 1F4 and 1F6 cells. Values are means \pm standard deviation. Asterisks represent a significant effect of 1F4 and 1F6 compared to the T-REx293 value ($P < 0.005$).**

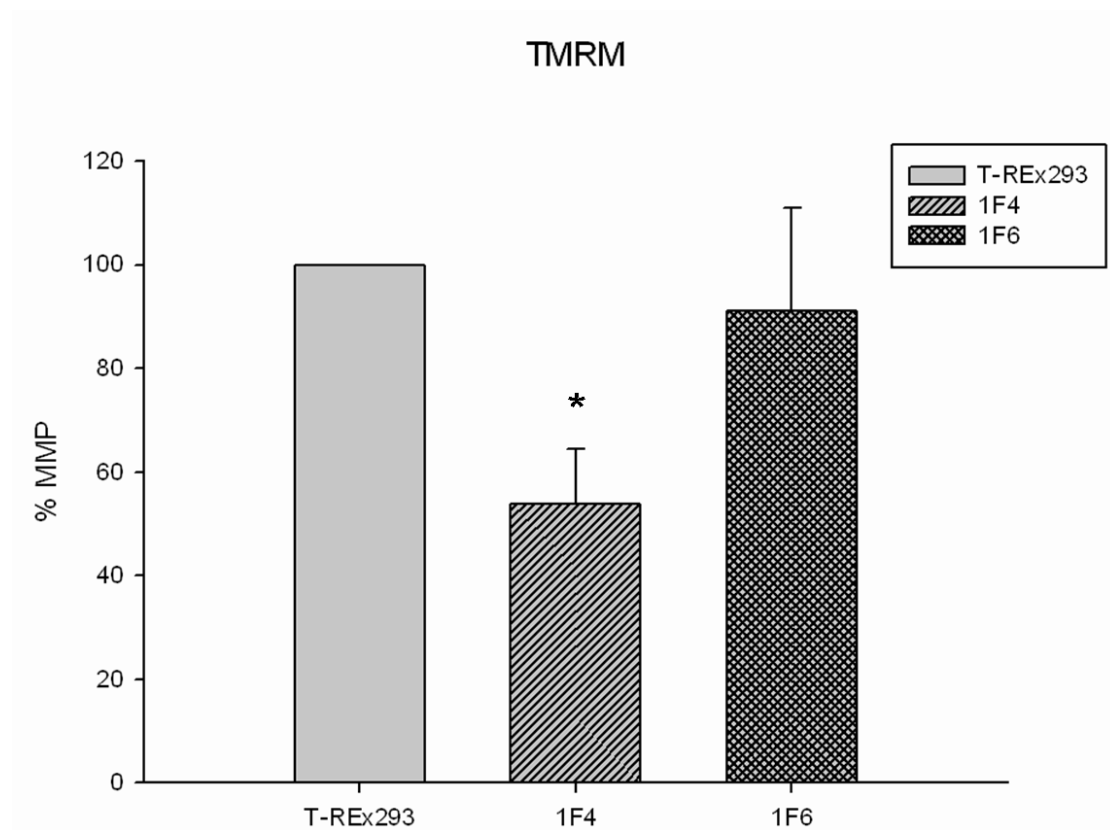


Figure 5. Mitochondrial membrane potential of T-REx293, 1F4 and 1F6 cells was measured by FACS. Mitochondrial membrane potential appeared red fluorescence using 200 nM TMRM staining for 20 min, and was measured by FL2 of FACScan flow cytometer. Values are means \pm standard deviation, and asterisks represent a significant effect of 1F4 and 1F6 compared to the T-REx293 value (**P* < 0.05).

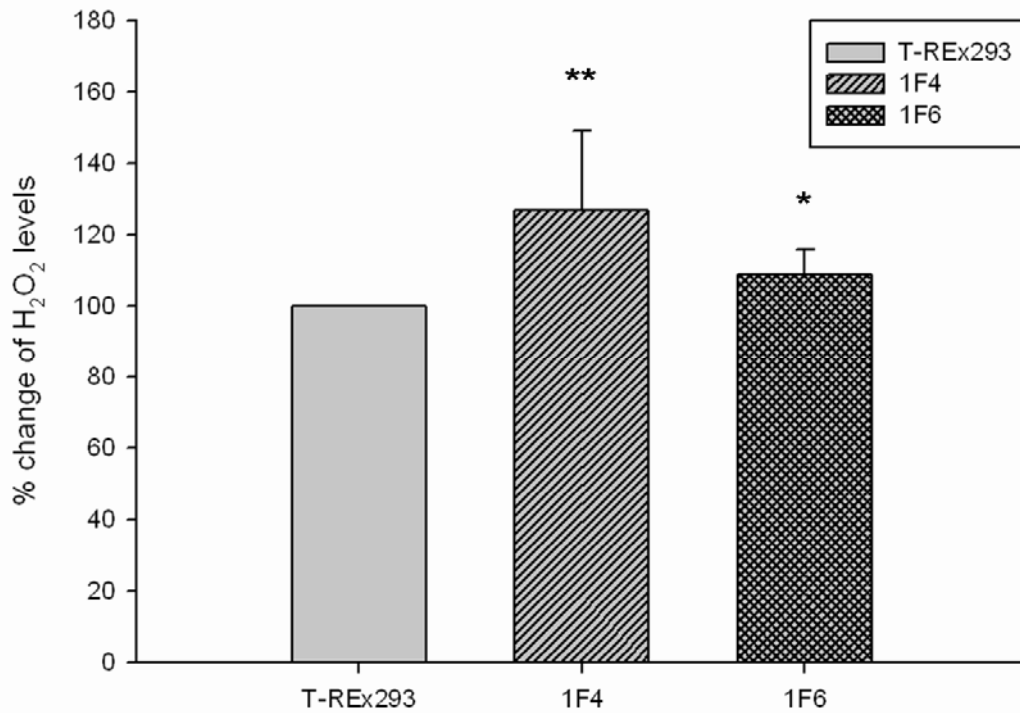


Figure 6. ROS generation assay detecting the H₂O₂ levels in T-REx293, 1F4 and 1F6 cells. Intracellular H₂O₂ appeared green fluorescence using 20 μ M DCFH-DA staining for 30 min, and was measured by FL1 of FACScan flow cytometer. Values are means \pm standard deviation. Asterisks represent a significant effect of 1F4 and 1F6 compared to the T-REx293 value (* P < 0.05, ** P < 0.005).

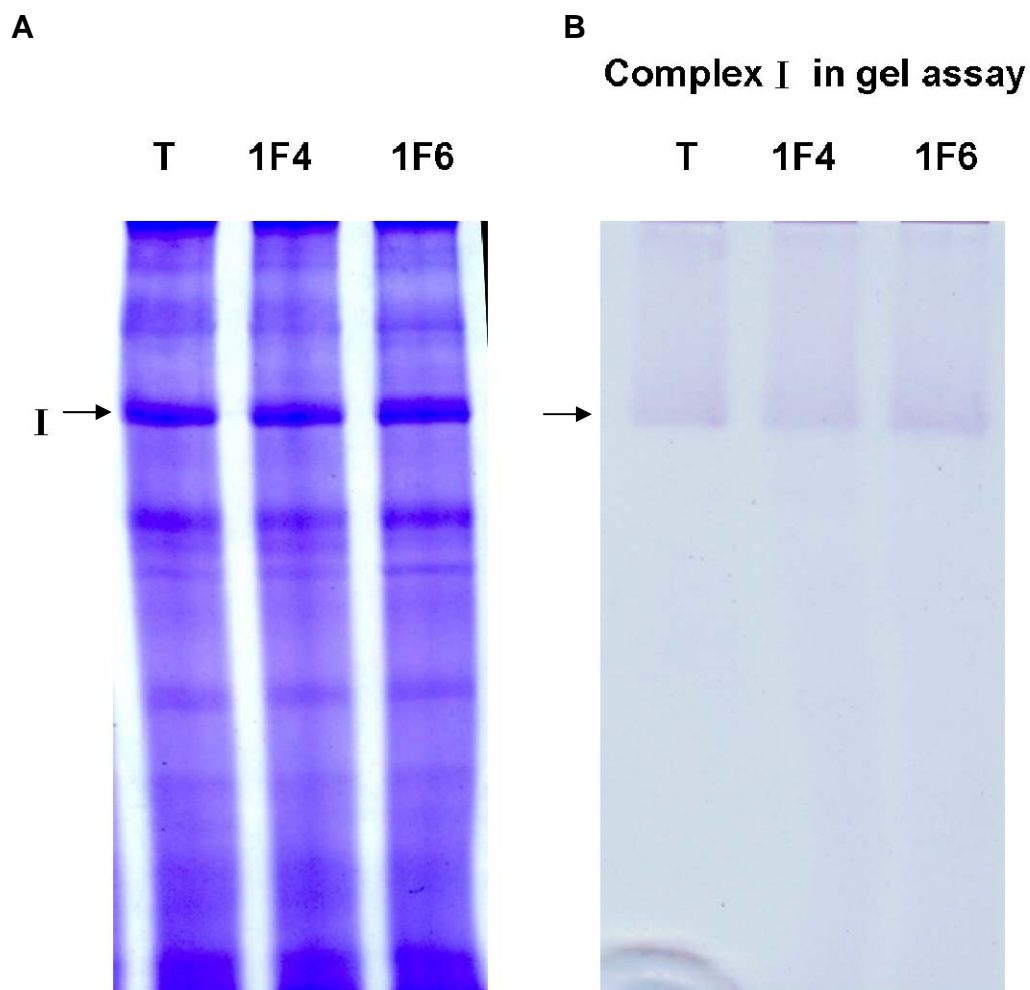
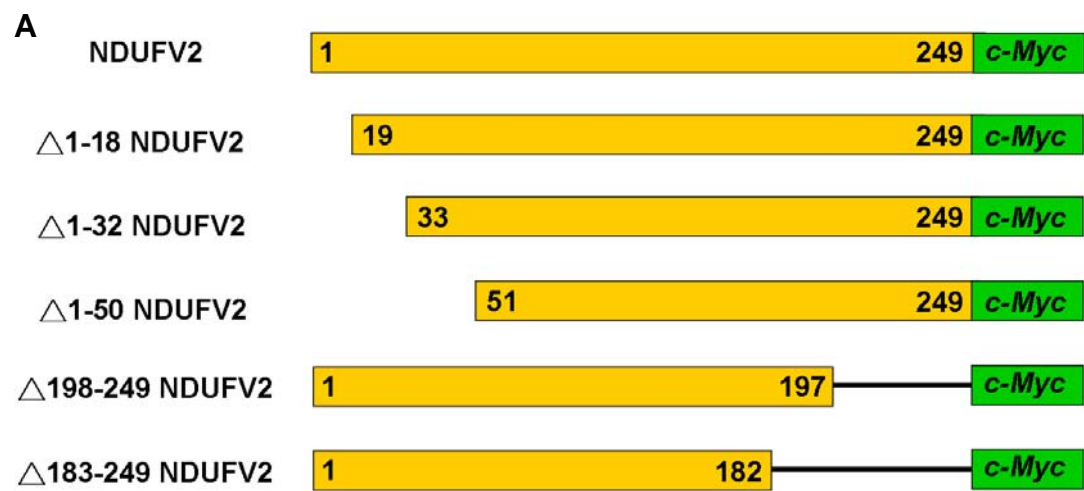


Figure 7. The hrCNE and complex I in gel assay were used to evaluate the assembly and activity of complex I. (A) The complex I-V assembly analyzed by coomassie blue staining. (B) The site of complex I activity was detected by complex I in gel assay.



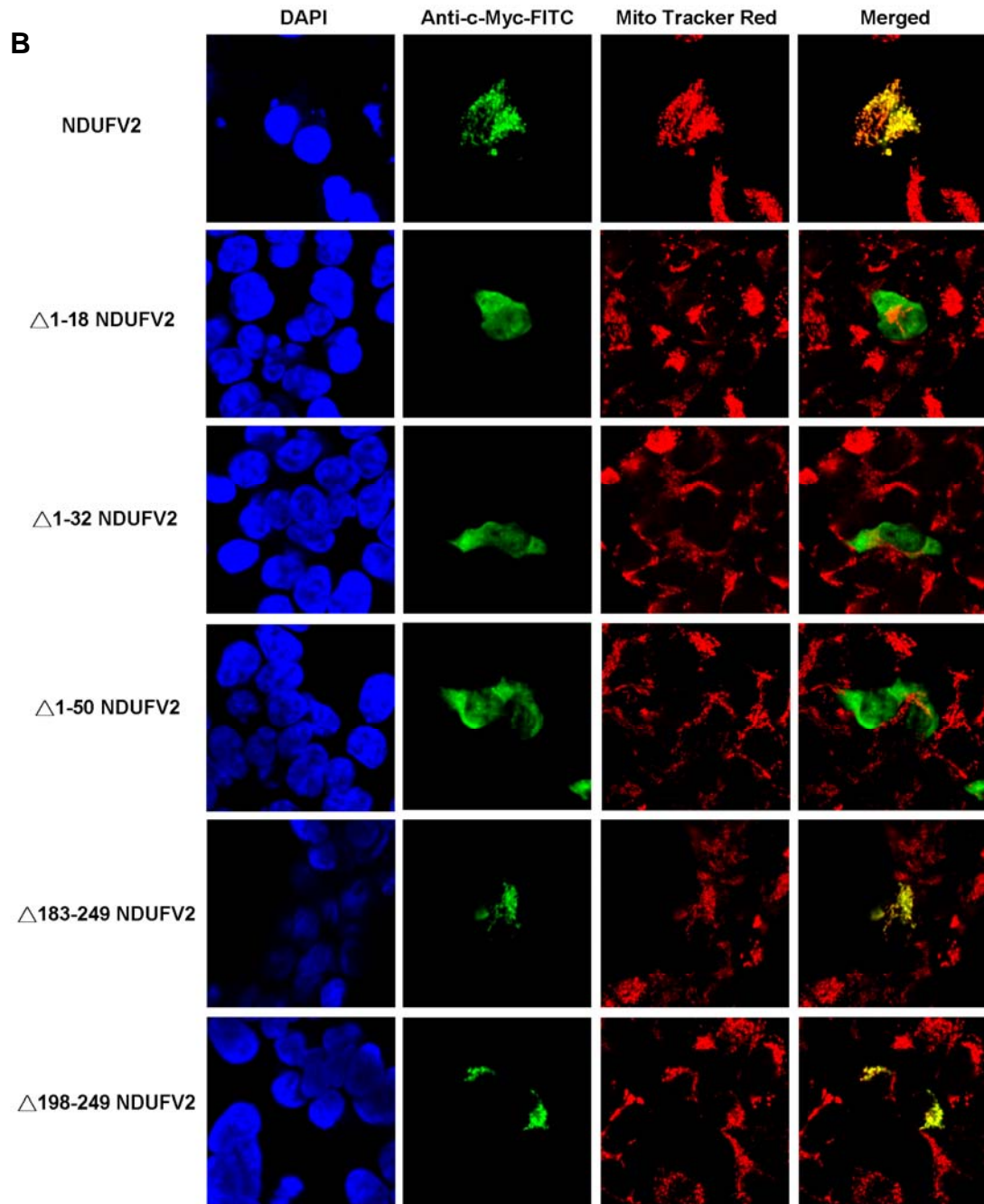


Figure 8. The effect of NDUFV2 N-terminal and C-terminal truncation on mitochondrial targeting. (A) The constructs expressing full-length and deleted NDUFV2 proteins. (B) The distribution of *c-myc* fusion proteins was detected by anti-*c-myc*-FITC antibody (green color). Blue color is nucleus labeled by DAPI and red color is mitochondria labeled by Mito Tracker Red.

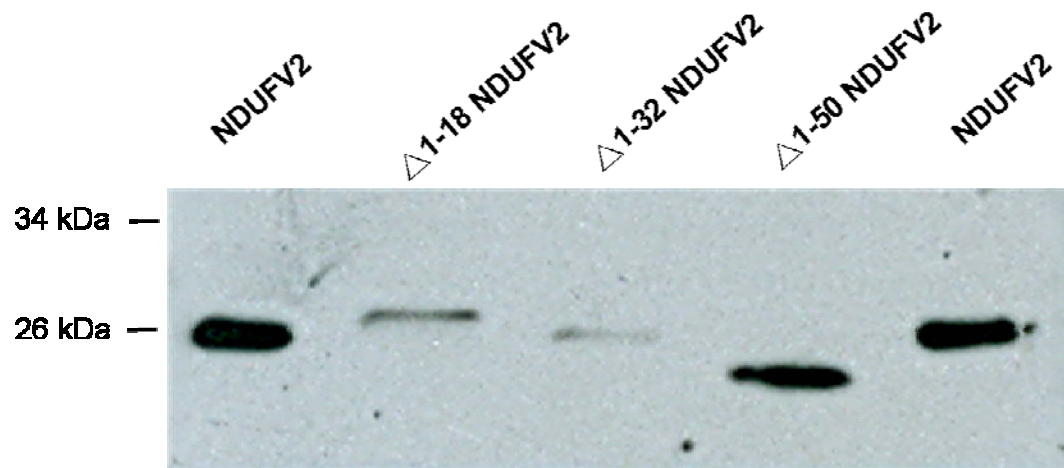
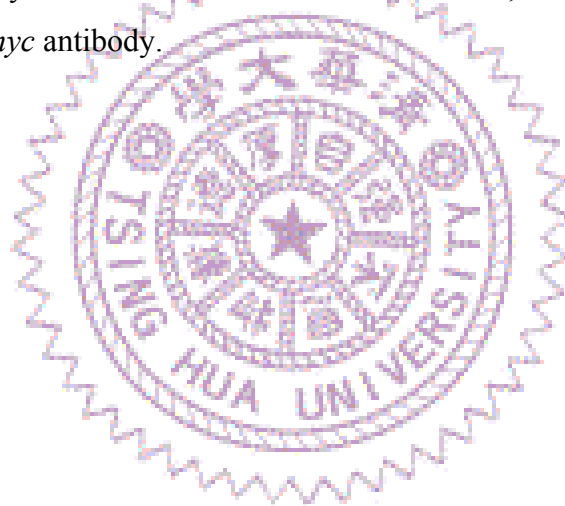
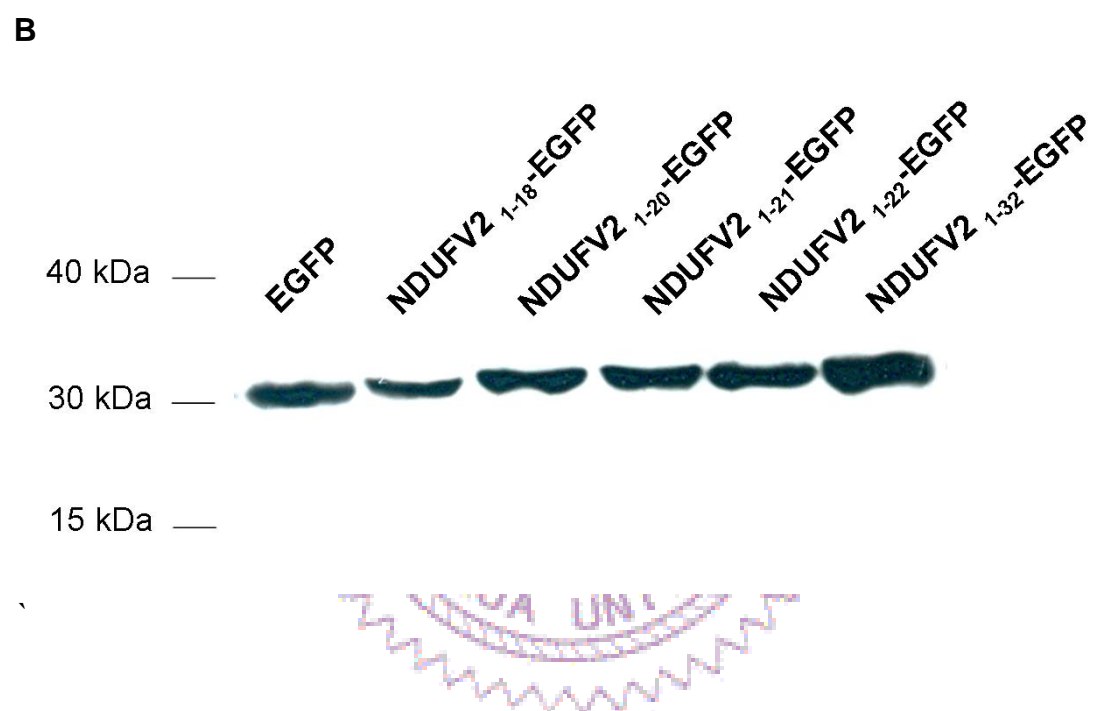
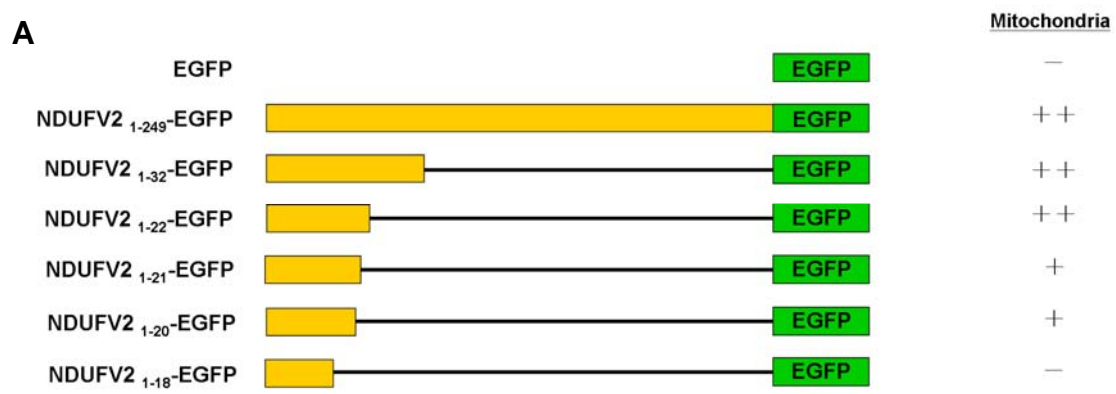


Figure 9. Cleavage site of the MTS occurs around residue 32 in the N-terminus of NDUFV2. Cell lysates were run on 15% SDS-PAGE, and blotted with mouse monoclonal anti-c-*myc* antibody.





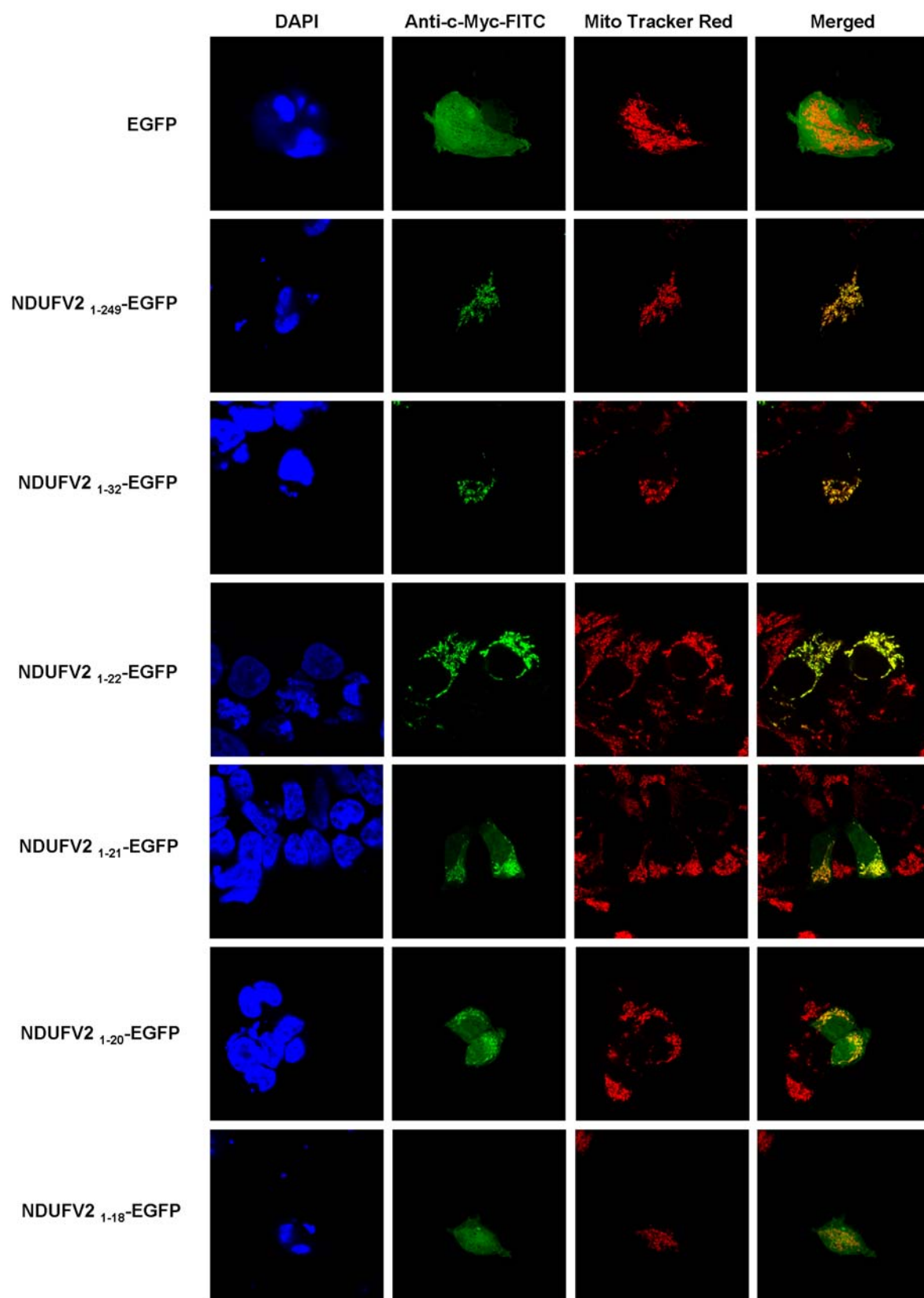


Figure 10. The first N-terminal 22 amino acids of NDUFV2 are sufficient to serve as a MTS for mitochondrial import. (A) The diagrammatic representation of EGFP fusion proteins carrying different lengths of NDUFV2 N-terminal peptides. (B) The protein expression of different lengths of NDUFV2 N-terminal peptides fusing with EGFP was checked by western blotting. Cell lysates were run on 10% SDS-PAGE, and blotted with mouse monoclonal anti-EGFP antibody. (C) The distribution of EGFP fusion proteins in transfected cells. Blue color is nucleus labeled by DAPI and red color is mitochondria labeled by Mito Tracker Red.



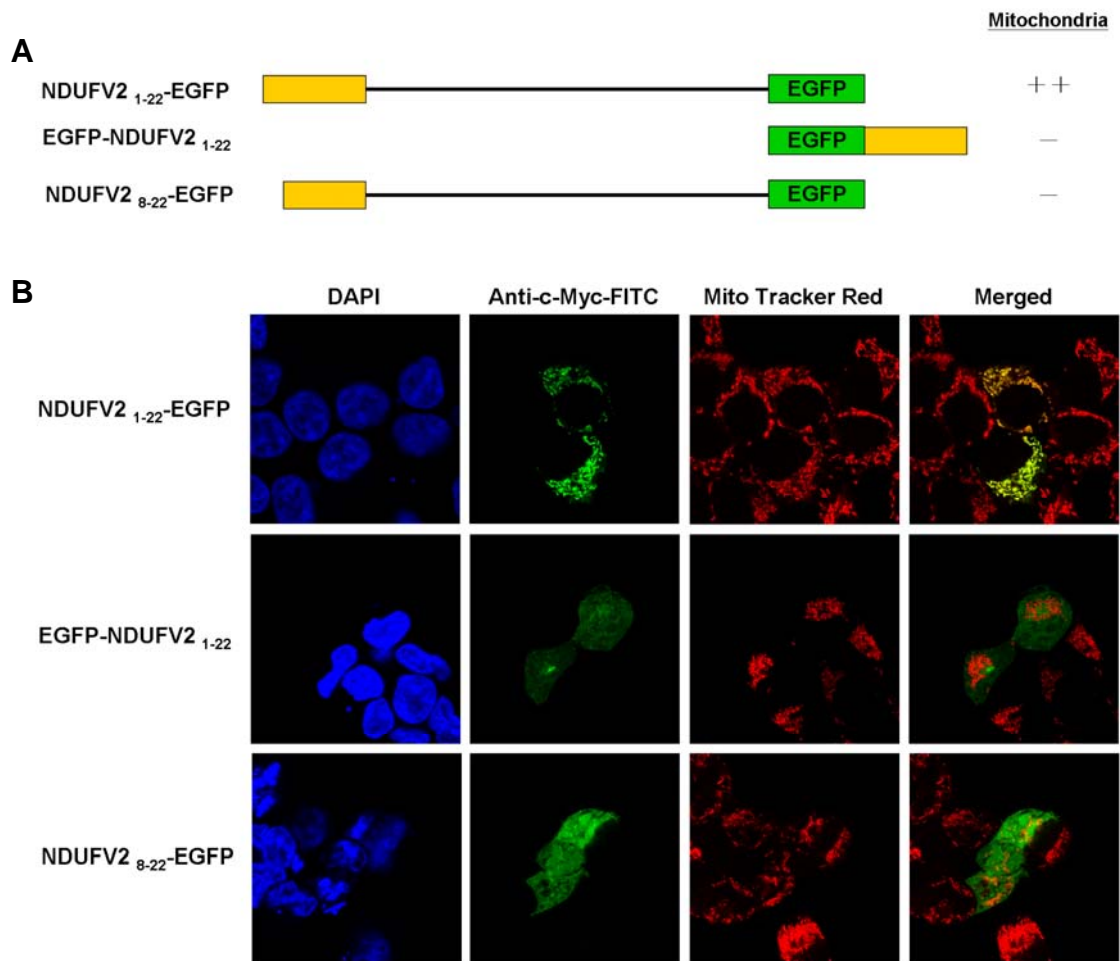












Figure 11. The MTS of NDUFV2 is directional for mitochondrial import. (A) The diagrammatic representation of EGFP fusion proteins. (B) The distribution of EGFP fusion proteins in transfected cells. Blue color is nucleus labeled by DAPI and red color is mitochondria labeled by Mito Tracker Red.



Conf: 
 Pred: 
 Pred: CCCCCCCCCCHHHHCCCCCHHHHHHHHHHHCCCCCCCCCCCC
 AA: MFFSAALRARAAGLTAHWGRHVRNLHKTVMQNGAGGALFV
 10 20 30 40



Conf: 
 Pred: 
 Pred: CCCCCCCCCCCCCCHHHHHHHHHHHHHHHHHCCCCCCHHHHH
 AA: HRDTPENNPDTPFDFTPENYKRIEAIKKNYPGHHKAAAVL
 50 60 70 80

Conf: 
 Pred: 
 Pred: HHHHHHHHHHCCCCCHHHHHHHHHHHHHCCCCCHHHHHHHHHCCCC
 AA: PVLDLAQRQNGWLPISAMNKVAEVLQVPPMRVYEVAFTYT
 90 100 110 120

Conf: 
 Pred: 
 Pred: CCCCCCCCCCEEEEEECCCHHHHHCCCHHHHHHHHHHHHHCCCC
 AA: MYNRKPVGKYHIQVCTTTPCMLRNSDSILEAIQKKGKIKV
 130 140 150 160

Conf: 
 Pred: 
 Pred: CCCCCCEEEEEEEECCECCCCCCCCCEEEECCEEECCCCCHHH
 AA: GETTPDKLFTLIEVECLGACVNAPMVQINDNYEDLTAKD
 170 180 190 200

Conf: 
 Pred: 
 Pred: HHHHHHHHHCCCCCCCCCCCCCCCCCCCCCCCCCCCCCCCCCCCC
 AA: IEEI IDELKAGKIPKPGPRSGRFSCEPAGGLTSLTEPPKG
 210 220 230 240

Conf: 
 Pred: 
 Pred: CCCHHHCCC
 AA: PGFGVQAGL

B

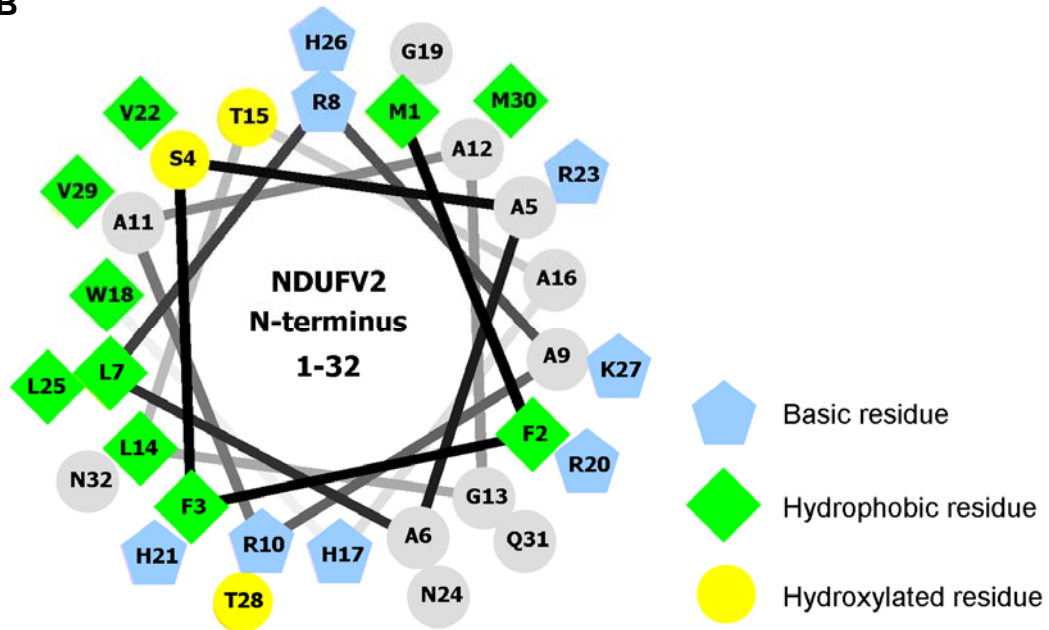


Figure 12. The prediction of secondary and tertiary structure of NDUFV2. Secondary structure of NDUFV2 was predicted by the PSIPRED server (<http://bioinf.cs.ucl.ac.uk/psipred/psiform.html>). (B) The α helical wheel diagram of the first 32 amino acids of NDUFV2 was constructed using program Helical Wheel Projections (<http://rnlab.ucr.edu/scripts/wheel/wheel.cgi>).

A 4 15 28

MFFSAALRARAAGLTAHWGRHVRNLHKTVMQN

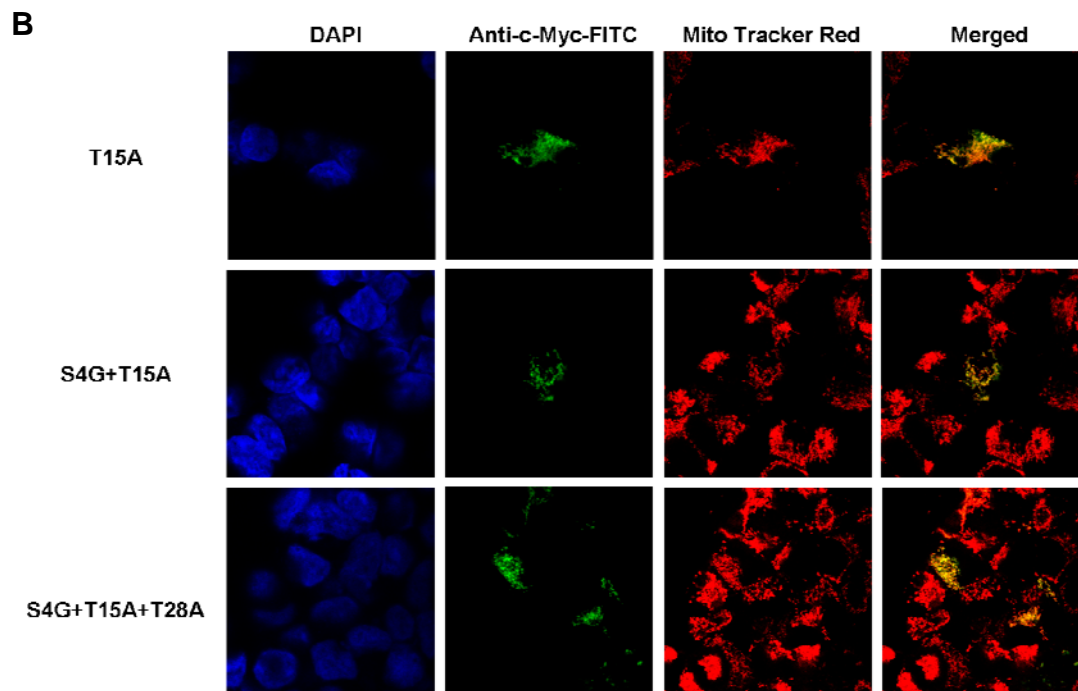


Figure 13. The effect of hydroxylated residue mutation in NDUFV2 MTS.

(A) The sites of the hydroxylated residue in NDUFV2 N-terminal 1-32 amino acids were marked. (B) The distribution of hydroxylated residue mutants were labeled by anti-c-*myc*-FITC antibody in transfected cells (green color). Blue color is nucleus labeled by DAPI and red color is mitochondria labeled by Mito Tracker Red.

A 8 10 17 2021 23 26 27

MFFSAALRARAAGLTAHWGRHVRNLHKTVMQN

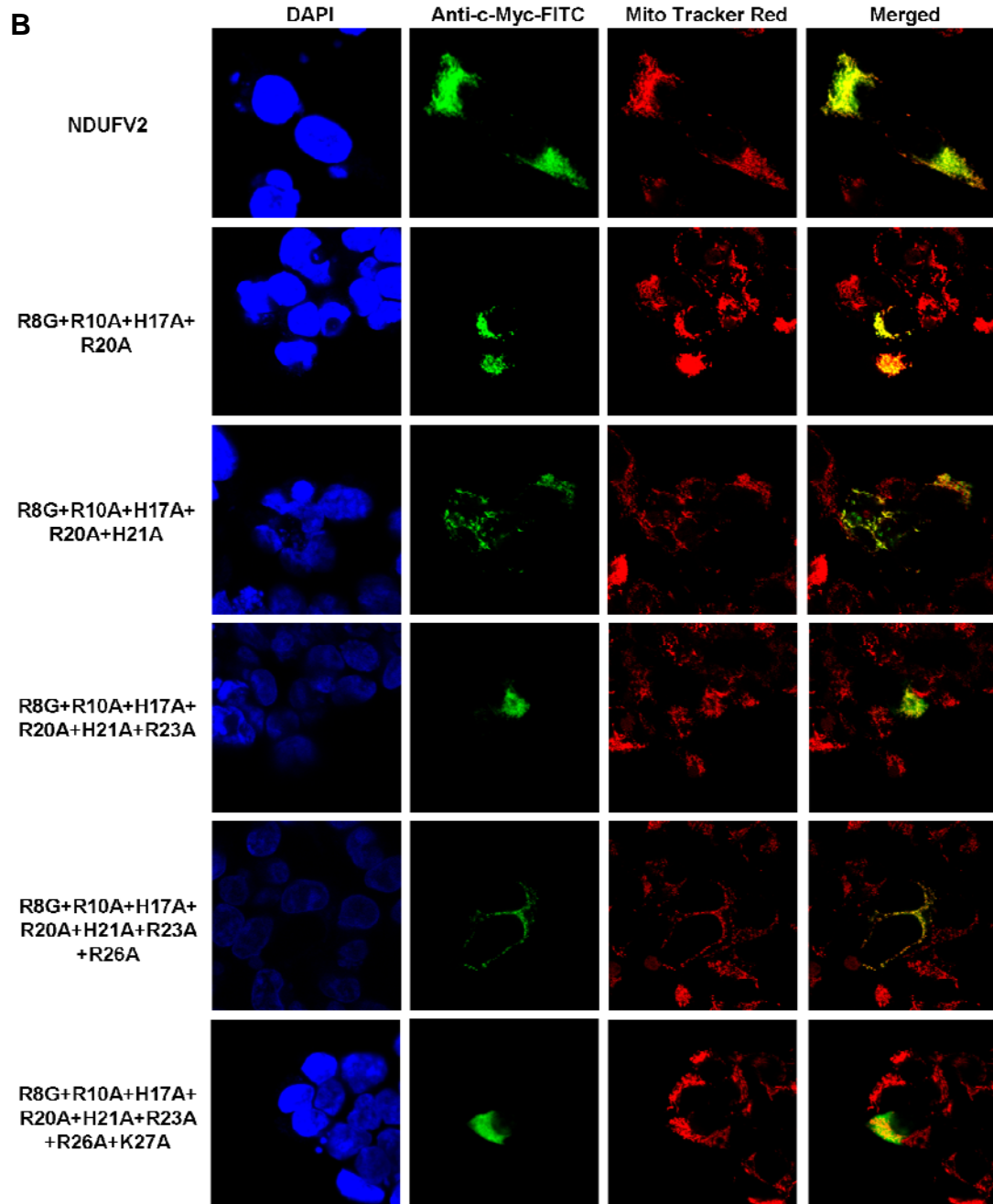


Figure 14. The effect of basic residue mutation in NDUFV2 MTS.

(A) The sites of the basic residue in NDUFV2 N-terminal 1-32 amino acids were marked. (B) The distribution of basic residue mutants were labeled by anti-c-*myc*-FITC antibody in transfected cells (green color). Blue color is nucleus labeled by DAPI and red color is mitochondria labeled by Mito Tracker Red.

A **23** **7** **14** **18** **22** **25** **29**

MFFSAALRARAAGLTAHWGRHVRNLHKTVMQN

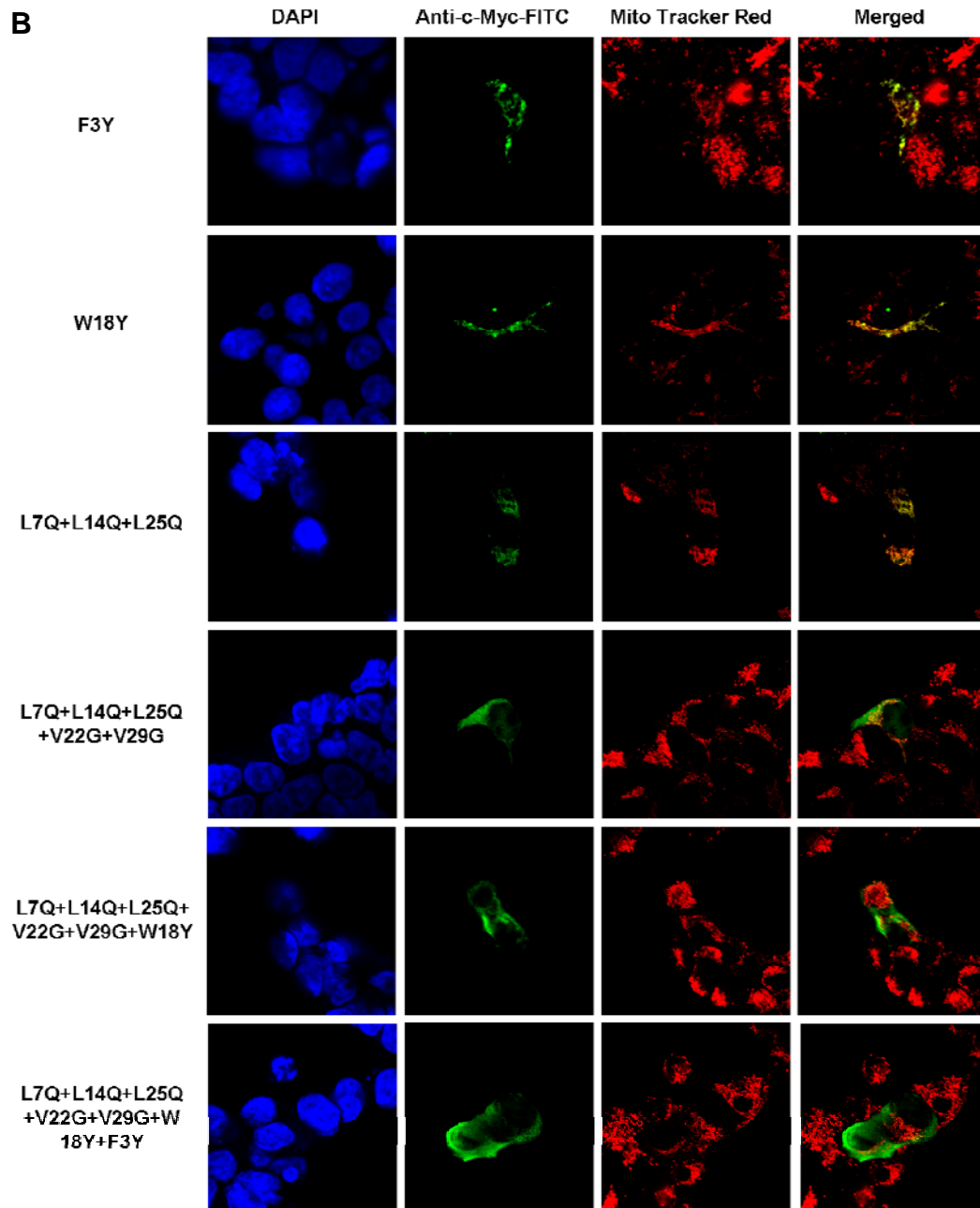


Figure 15. The effect of hydrophobic residue mutation in NDUFV2 MTS.

(A) The sites of the hydrophobic residue in NDUFV2 N-terminal 1-32 amino acids were marked. (B) The distribution of hydrophobic residue mutants were labeled by anti-c-myc-FITC antibody in transfected cells (green color). Blue color is nucleus labeled by DAPI and red color is mitochondria labeled by Mito Tracker Red.

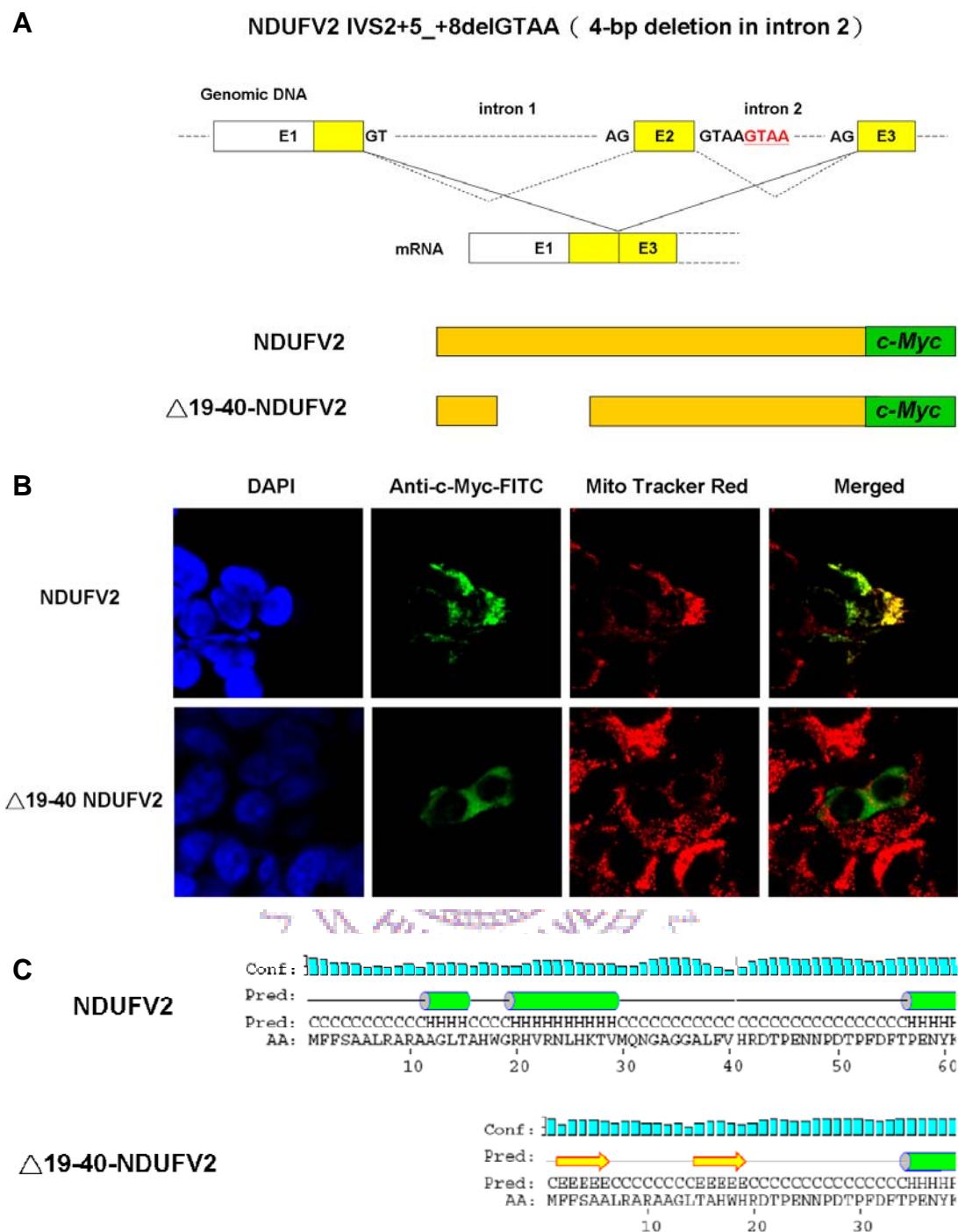
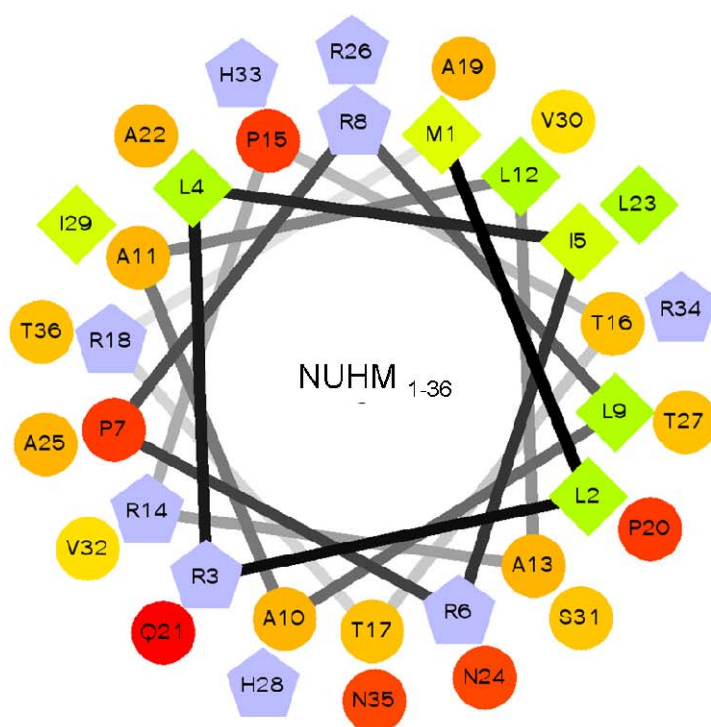


Figure 16. Establish the human early-onset hypertrophic cardiomyopathy and encephalopathy disease model. (A) Genomic structure of NDUFV2 (exon 1-3). Dotted line indicates wild-type splicing form; Continuous line indicates abnormal splicing form. (B) The constructs and protein distributed patterns of wild-type and NDUFV2 deletion mutant. (C) The secondary structure prediction of wild-type and NDUFV2 mutant.

A



B

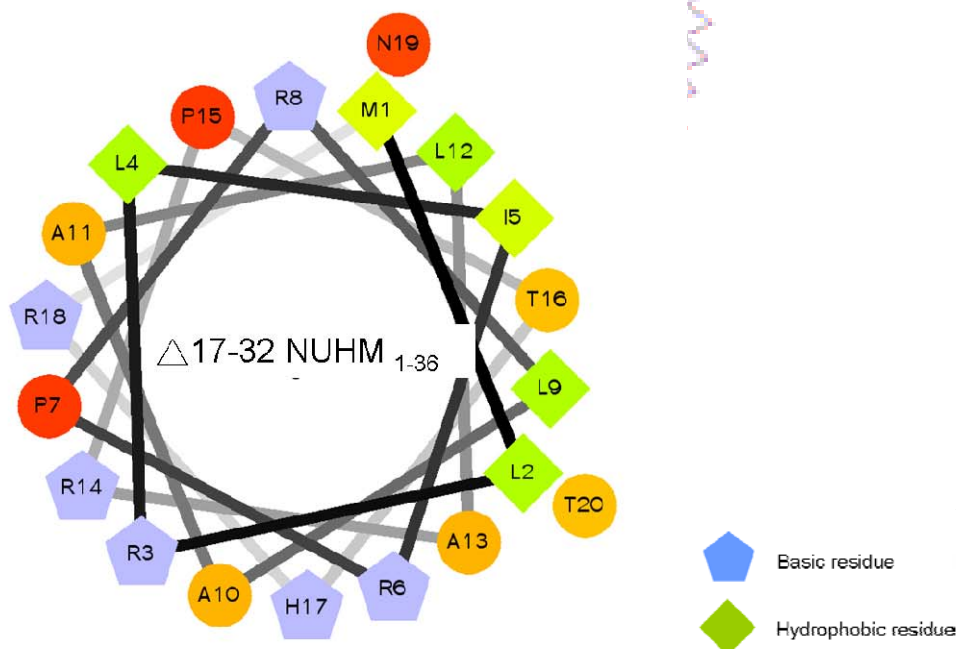


Figure 17. The prediction patterns of α helical wheel in NUHM₁₋₃₆ and truncated NUHM mutant. The α helical wheel diagram of the first 36 amino acids of wild type NUHM (A) and truncated mutant (B) were constructed using program Helical Wheel Projections ([http:// rzlab. ucr. edu/ scripts/ wheel/ wheel. cgi](http://rzlab.ucr.edu/scripts/wheel/wheel.cgi)).

References

1. Brown GC: **Control of respiration and ATP synthesis in mammalian mitochondria and cells.** *Biochem J* 1992, **284** (Pt 1):1-13.
2. Hatefi Y: **The mitochondrial electron transport and oxidative phosphorylation system.** *Annu Rev Biochem* 1985, **54**:1015-1069.
3. Taanman JW: **The mitochondrial genome: structure, transcription, translation and replication.** *Biochim Biophys Acta* 1999, **1410**(2):103-123.
4. Wallace DC: **The mitochondrial genome in human adaptive radiation and disease: on the road to therapeutics and performance enhancement.** *Gene* 2005, **354**:169-180.
5. Balaban RS, Nemoto S, Finkel T: **Mitochondria, oxidants, and aging.** *Cell* 2005, **120**(4):483-495.
6. Huang H, Manton KG: **The role of oxidative damage in mitochondria during aging: a review.** *Front Biosci* 2004, **9**:1100-1117.
7. Lynn S, Wardell T, Johnson MA, Chinnery PF, Daly ME, Walker M, Turnbull DM: **Mitochondrial diabetes: investigation and identification of a novel mutation.** *Diabetes* 1998, **47**(11):1800-1802.
8. Wallace DC: **A mitochondrial paradigm of metabolic and degenerative diseases, aging, and cancer: a dawn for evolutionary medicine.** *Annu Rev Genet* 2005, **39**:359-407.
9. Wallace DC: **Why do we still have a maternally inherited mitochondrial DNA? Insights from evolutionary medicine.** *Annu Rev Biochem* 2007, **76**:781-821.
10. Bolender N, Sickmann A, Wagner R, Meisinger C, Pfanner N: **Multiple pathways for sorting mitochondrial precursor proteins.** *EMBO Rep* 2008, **9**(1):42-49.
11. Horwich AL, Kalousek F, Mellman I, Rosenberg LE: **A leader peptide is sufficient to direct mitochondrial import of a chimeric protein.** *EMBO J* 1985, **4**(5):1129-1135.
12. von Heijne G: **A new method for predicting signal sequence cleavage sites.** *Nucleic Acids Res* 1986, **14**(11):4683-4690.
13. Gavel Y, von Heijne G: **Cleavage-site motifs in mitochondrial targeting peptides.** *Protein Eng* 1990, **4**(1):33-37.
14. Lenaz G, Fato R, Baracca A, Genova ML: **Mitochondrial quinone reductases: complex I.** *Methods Enzymol* 2004, **382**:3-20.

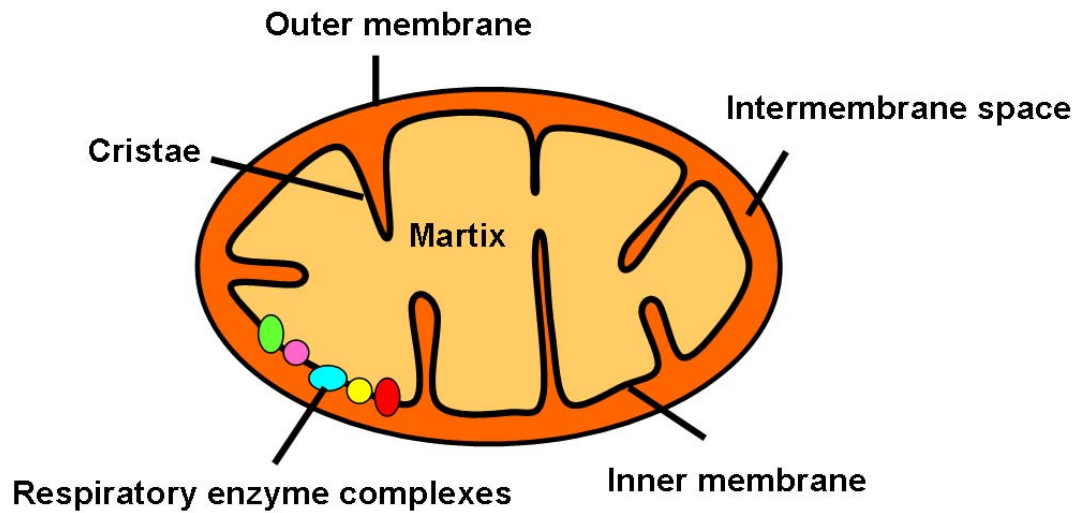
15. Bai Y, Hu P, Park JS, Deng JH, Song X, Chomyn A, Yagi T, Attardi G: **Genetic and functional analysis of mitochondrial DNA-encoded complex I genes.** *Ann N Y Acad Sci* 2004, **1011**:272-283.
16. Grigorieff N: **Structure of the respiratory NADH:ubiquinone oxidoreductase (complex I).** *Curr Opin Struct Biol* 1999, **9**(4):476-483.
17. Friedrich T, Bottcher B: **The gross structure of the respiratory complex I: a Lego System.** *Biochim Biophys Acta* 2004, **1608**(1):1-9.
18. Scheffler IE, Yadava N, Potluri P: **Molecular genetics of complex I-deficient Chinese hamster cell lines.** *Biochim Biophys Acta* 2004, **1659**(2-3):160-171.
19. Carroll J, Fearnley IM, Shannon RJ, Hirst J, Walker JE: **Analysis of the subunit composition of complex I from bovine heart mitochondria.** *Mol Cell Proteomics* 2003, **2**(2):117-126.
20. Smeitink JA, Loeffen JL, Triepels RH, Smeets RJ, Trijbels JM, van den Heuvel LP: **Nuclear genes of human complex I of the mitochondrial electron transport chain: state of the art.** *Hum Mol Genet* 1998, **7**(10):1573-1579.
21. Saraste M: **Oxidative phosphorylation at the fin de siecle.** *Science* 1999, **283**(5407):1488-1493.
22. Schultz BE, Chan SI: **Structures and proton-pumping strategies of mitochondrial respiratory enzymes.** *Annu Rev Biophys Biomol Struct* 2001, **30**:23-65.
23. Sled VD, Friedrich T, Leif H, Weiss H, Meinhardt SW, Fukumori Y, Calhoun MW, Gennis RB, Ohnishi T: **Bacterial NADH-quinone oxidoreductases: iron-sulfur clusters and related problems.** *J Bioenerg Biomembr* 1993, **25**(4):347-356.
24. Ohnishi T: **Iron-sulfur clusters/semiquinones in complex I.** *Biochim Biophys Acta* 1998, **1364**(2):186-206.
25. Yano T, Yagi T: **H(+)-translocating NADH-quinone oxidoreductase (NDH-1) of Paracoccus denitrificans. Studies on topology and stoichiometry of the peripheral subunits.** *J Biol Chem* 1999, **274**(40):28606-28611.
26. Hinchliffe P, Sazanov LA: **Organization of iron-sulfur clusters in respiratory complex I.** *Science* 2005, **309**(5735):771-774.
27. Brandt U: **Energy converting NADH:quinone oxidoreductase (complex I).** *Annu Rev Biochem* 2006, **75**:69-92.
28. de Coo R, Buddiger P, Smeets H, Geurts van Kessel A, Morgan-Hughes J, Weghuis DO, Overhauser J, van Oost B: **Molecular cloning and characterization of the active human mitochondrial NADH:ubiquinone**

- oxidoreductase 24-kDa gene (NDUFV2) and its pseudogene. *Genomics* 1995, **26**(3):461-466.
29. Hattori N: **Structural organization and chromosomal localization of the human nuclear gene (NDUFV2) for the 24-kDa iron-sulfur subunit of complex I in mitochondrial respiratory chain.pdf.** *biochemical and biophysical research communications* 1995, **216**:771-777.
30. Weidner U, Geier S, Ptock A, Friedrich T, Leif H, Weiss H: **The gene locus of the proton-translocating NADH: ubiquinone oxidoreductase in Escherichia coli. Organization of the 14 genes and relationship between the derived proteins and subunits of mitochondrial complex I.** *J Mol Biol* 1993, **233**(1):109-122.
31. Duborjal H, Dupuis A, Chapel A, Kieffer S, Lunardi J, Issartel JP: **Immuno-purification of a dimeric subcomplex of the respiratory NADH-CoQ reductase of Rhodobacter capsulatus equivalent to the FP fraction of the mitochondrial complex I.** *FEBS Lett* 1997, **405**(3):345-350.
32. Yano T, Sled VD, Ohnishi T, Yagi T: **Expression of the 25-kilodalton iron-sulfur subunit of the energy-transducing NADH-ubiquinone oxidoreductase of Paracoccus denitrificans.** *Biochemistry* 1994, **33**(2):494-499.
33. Yano T, Chu SS, Sled VD, Ohnishi T, Yagi T: **The proton-translocating NADH-quinone oxidoreductase (NDH-1) of thermophilic bacterium Thermus thermophilus HB-8. Complete DNA sequence of the gene cluster and thermostable properties of the expressed NQO2 subunit.** *J Biol Chem* 1997, **272**(7):4201-4211.
34. Almeida T, Duarte M, Melo AM, Videira A: **The 24-kDa iron-sulphur subunit of complex I is required for enzyme activity.** *Eur J Biochem* 1999, **265**(1):86-93.
35. Kerscher S, Benit P, Abdrakhmanova A, Zwicker K, Rais I, Karas M, Rustin P, Brandt U: **Processing of the 24 kDa subunit mitochondrial import signal is not required for assembly of functional complex I in Yarrowia lipolytica.** *Eur J Biochem* 2004, **271**(17):3588-3595.
36. Velazquez I, Nakamaru-Ogiso E, Yano T, Ohnishi T, Yagi T: **Amino acid residues associated with cluster N3 in the NuoF subunit of the proton-translocating NADH-quinone oxidoreductase from Escherichia coli.** *FEBS Lett* 2005, **579**(14):3164-3168.
37. Friedrich T: **The NADH:ubiquinone oxidoreductase (complex I) from Escherichia coli.** *Biochim Biophys Acta* 1998, **1364**(2):134-146.
38. Yagi T, Dinh TM: **Identification of the NADH-binding subunit of**

- NADH-ubiquinone oxidoreductase of *Paracoccus denitrificans*.** *Biochemistry* 1990, **29**(23):5515-5520.
39. Yano T, Sled VD, Ohnishi T, Yagi T: **Expression and characterization of the flavoprotein subcomplex composed of 50-kDa (NQO1) and 25-kDa (NQO2) subunits of the proton-translocating NADH-quinone oxidoreductase of *Paracoccus denitrificans*.** *J Biol Chem* 1996, **271**(10):5907-5913.
40. Yano T, Sled VD, Ohnishi T, Yagi T: **Identification of amino acid residues associated with the [2Fe-2S] cluster of the 25 kDa (NQO2) subunit of the proton-translocating NADH-quinone oxidoreductase of *Paracoccus denitrificans*.** *FEBS Lett* 1994, **354**(2):160-164.
41. Zu Y, Di Bernardo S, Yagi T, Hirst J: **Redox properties of the [2Fe-2S] center in the 24 kDa (NQO2) subunit of NADH:ubiquinone oxidoreductase (complex I).** *Biochemistry* 2002, **41**(31):10056-10069.
42. Sazanov LA, Hinchliffe P: **Structure of the hydrophilic domain of respiratory complex I from *Thermus thermophilus*.** *Science* 2006, **311**(5766):1430-1436.
43. Videira A: **Complex I from the fungus *Neurospora crassa*.** *Biochim Biophys Acta* 1998, **1364**(2):89-100.
44. von Bahr-Lindstrom H, Galante YM, Persson M, Jornvall H: **The primary structure of subunit II of NADH dehydrogenase from bovine-heart mitochondria.** *Eur J Biochem* 1983, **134**(1):145-150.
45. Pilkington SJ, Walker JE: **Mitochondrial NADH-ubiquinone reductase: complementary DNA sequences of import precursors of the bovine and human 24-kDa subunit.** *Biochemistry* 1989, **28**(8):3257-3264.
46. Hattori N, Yoshino H, Tanaka M, Suzuki H, Mizuno Y: **Genotype in the 24-kDa subunit gene (NDUFV2) of mitochondrial complex I and susceptibility to Parkinson disease.** *Genomics* 1998, **49**(1):52-58.
47. Kim SH, Vlkolinsky R, Cairns N, Fountoulakis M, Lubec G: **The reduction of NADH ubiquinone oxidoreductase 24- and 75-kDa subunits in brains of patients with Down syndrome and Alzheimer's disease.** *Life Sci* 2001, **68**(24):2741-2750.
48. Karry R, Klein E, Ben Shachar D: **Mitochondrial complex I subunits expression is altered in schizophrenia: a postmortem study.** *Biol Psychiatry* 2004, **55**(7):676-684.
49. Nakatani N, Hattori E, Ohnishi T, Dean B, Iwayama Y, Matsumoto I, Kato T, Osumi N, Higuchi T, Niwa S *et al*: **Genome-wide expression analysis detects eight genes with robust alterations specific to bipolar I disorder:**

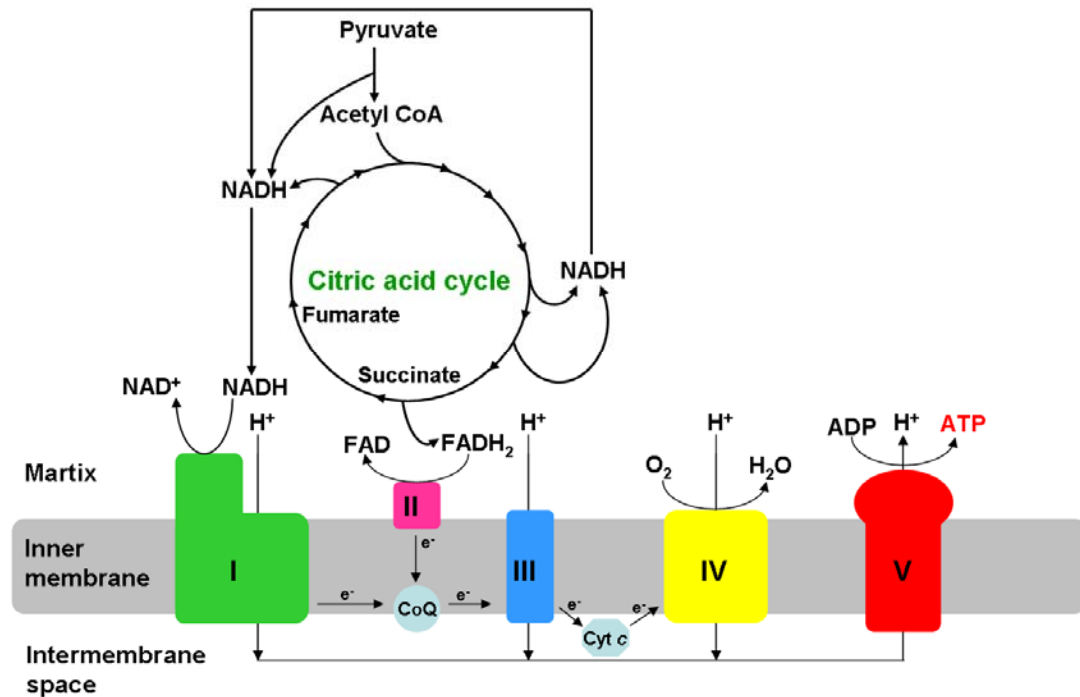
- relevance to neuronal network perturbation.** *Hum Mol Genet* 2006, **15**(12):1949-1962.
50. Loeffen J, Elpeleg O, Smeitink J, Smeets R, Stockler-Ipsiroglu S, Mandel H, Sengers R, Trijbels F, van den Heuvel L: **Mutations in the complex I NDUFS2 gene of patients with cardiomyopathy and encephalomyopathy.** *Ann Neurol* 2001, **49**(2):195-201.
51. Benit P, Beugnot R, Chretien D, Giurgea I, De Lonlay-Debeney P, Issartel JP, Corral-Debrinski M, Kerscher S, Rustin P, Rotig A *et al*: **Mutant NDUFV2 subunit of mitochondrial complex I causes early onset hypertrophic cardiomyopathy and encephalopathy.** *Hum Mutat* 2003, **21**(6):582-586.
52. Djafarzadeh R, Kerscher S, Zwicker K, Radermacher M, Lindahl M, Schagger H, Brandt U: **Biophysical and structural characterization of proton-translocating NADH-dehydrogenase (complex I) from the strictly aerobic yeast *Yarrowia lipolytica*.** *Biochim Biophys Acta* 2000, **1459**(1):230-238.
53. Barrientos A: **In vivo and in organello assessment of OXPHOS activities.** *Methods* 2002, **26**(4):307-316.
54. Weiss H, von Jagow G, Klingenberg M, Bucher T: **Characterization of *Neurospora crassa* mitochondria prepared with a grind-mill.** *Eur J Biochem* 1970, **14**(1):75-82.
55. Kerscher S, Droese S, Zickermann V, Brandt U: **The three families of respiratory NADH dehydrogenases.** *Results Probl Cell Differ* 2008, **45**:185-222.
56. Sabherwal N, Schneider KU, Blaschke RJ, Marchini A, Rappold G: **Impairment of SHOX nuclear localization as a cause for Leri-Weill syndrome.** *J Cell Sci* 2004, **117**(Pt 14):3041-3048.
57. Claypool SM, McCaffery JM, Koehler CM: **Mitochondrial mislocalization and altered assembly of a cluster of Barth syndrome mutant tafazzins.** *J Cell Biol* 2006, **174**(3):379-390.

Appendixes

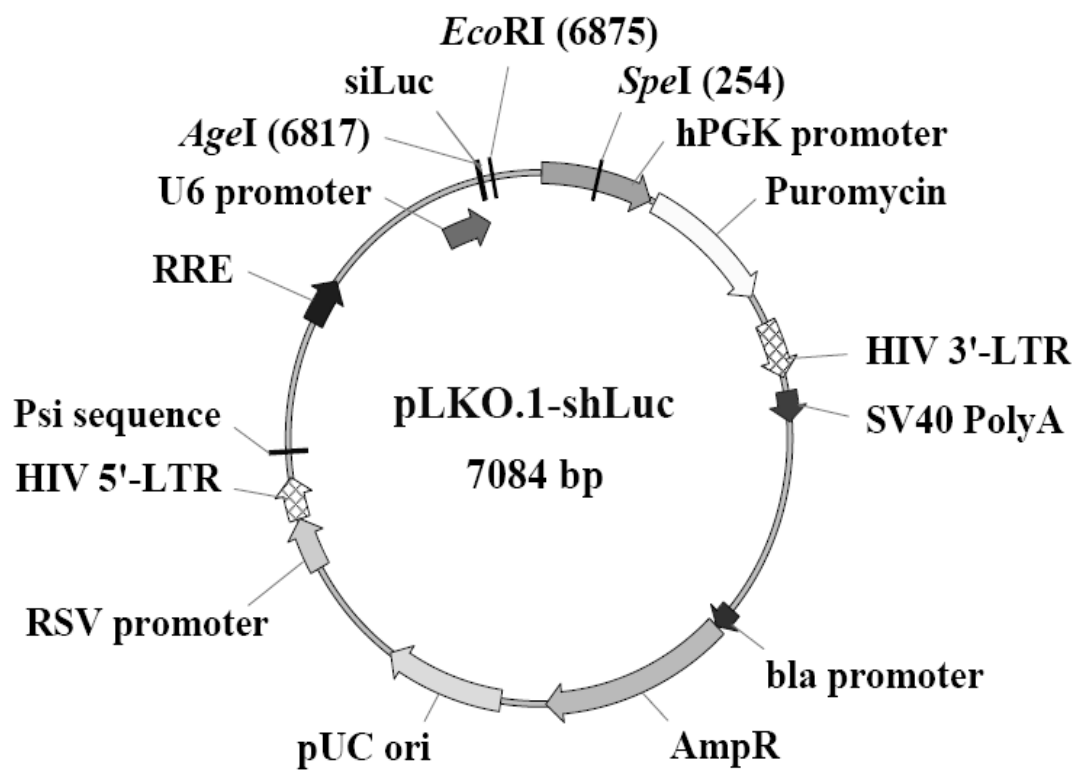


Appendix 1. The structure of mitochondria

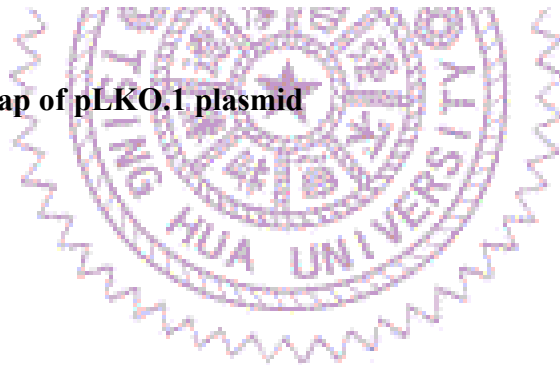


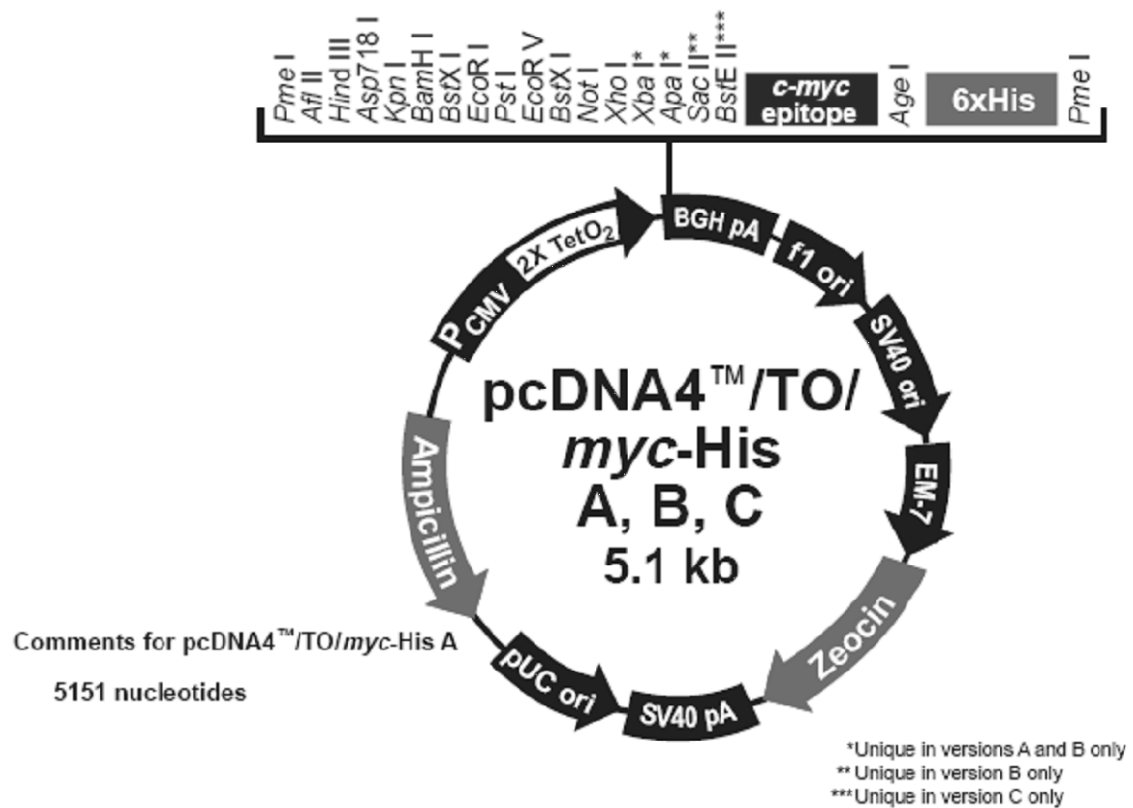


Appendix 2. Mammalian mitochondrial electron transport chain (ETC) and oxidative phosphorylation system (OXPHOS). The OXPHOS includes NADH-ubiquinone oxidoreductase (complex I), succinate- ubiquinone oxidoreductase (complex II), ubiquinol-cytochrome *c* oxidoreductase (complex III), cytochrome *c* oxidase (complex IV), ATP synthase (complex V), ubiquinone (CoQ) and cytochrome *c* (Cyt *c*).

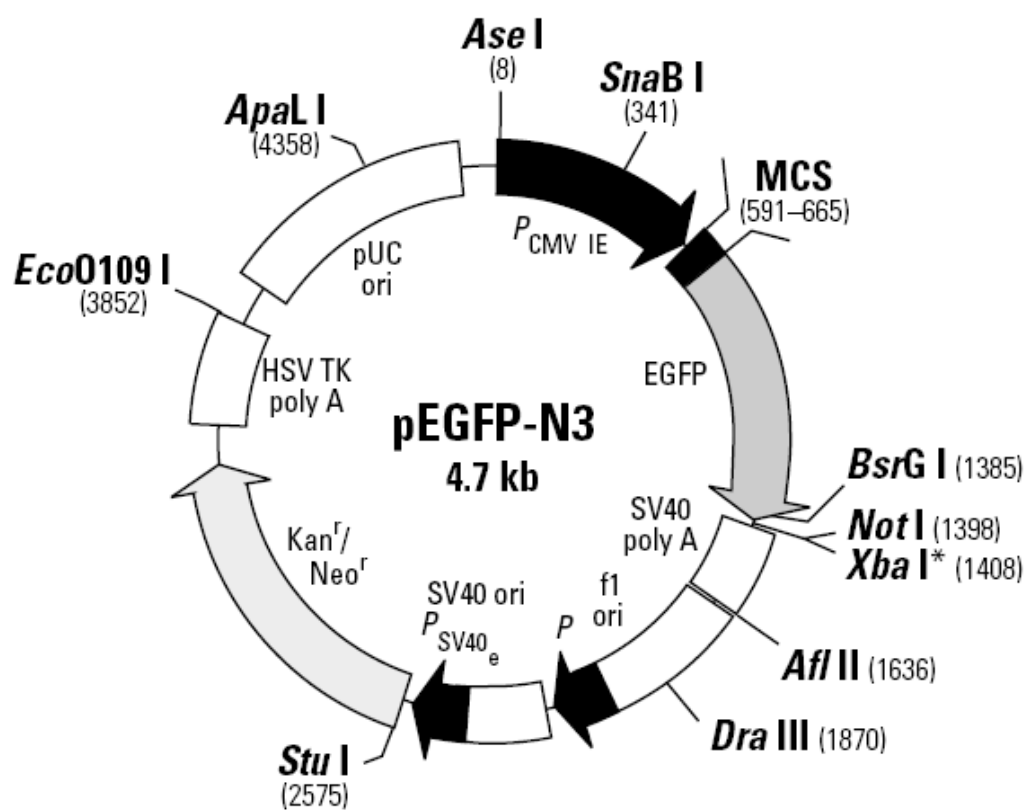


Appendix 3. The map of pLKO.1 plasmid





Appendix 4. The map of pcDNA4™/TO/myc-His A plasmid



Appendix 5. The map of pEGFP-N3

